

St. John's University

St. John's Scholar

Theses and Dissertations

2023

**HYDROXYUREA GLOBALLY INHIBITS RNA SYNTHESIS,
DESTABILIZES mRNAs, AND TRIGGERS MEC1-OPPOSED RNAPII
ACCUMULATION AT 3' ENDS OF GENES**

Pritpal Kaur

Follow this and additional works at: https://scholar.stjohns.edu/theses_dissertations



Part of the **Biology Commons**

HYDROXYUREA GLOBALLY INHIBITS RNA SYNTHESIS, DESTABILIZES
mRNAs, AND TRIGGERS MEC1-OPPOSED RNAPII ACCUMULATION AT 3'
ENDS OF GENES

A dissertation submitted in partial fulfillment
of the requirements for the degree of

DOCTOR OF PHILOSOPHY

to the faculty of the

DEPARTMENT OF BIOLOGICAL SCIENCES

of

ST. JOHN'S COLLEGE OF LIBERAL ARTS AND SCIENCES

at

ST. JOHN'S UNIVERSITY

New York

by

Pritpal Kaur

Date Submitted 11/10/2022

Date Approved 12/21/2022

Pritpal Kaur

Dr. Ales Vancura

© Copyright by Pritpal Kaur 2023

All Rights Reserved

ABSTRACT

HYDROXYUREA GLOBALLY INHIBITS RNA SYNTHESIS, DESTABILIZES mRNAs, AND TRIGGERS MEC1-OPPOSED RNAPII ACCUMULATION AT 3' ENDS OF GENES

Pritpal Kaur

My dissertation includes two projects. The first project focused on regulation of glycolysis and oxidative metabolism by inducing heme synthesis in cancer cells. Heme is an essential cofactor for enzymes of the electron transport chain (ETC) and ATP synthesis in mitochondrial oxidative phosphorylation (OXPHOS). Heme also binds to and destabilizes Bach1, a transcription regulator that controls expression of several groups of genes important for glycolysis, ETC, and metastasis of cancer cells. Many cancers are characterized by a high glycolytic rate, targeting glycolysis, ETC, and OXPHOS have emerged as a potential therapeutic strategy. Here, we report that enhancing heme synthesis through exogenous supplementation of heme precursor 5-aminolevulinic acid (ALA) suppresses oxidative metabolism as well as glycolysis and significantly reduces proliferation of both ovarian and breast cancer cells. ALA supplementation also destabilizes Bach1 and inhibits migration of both cell types. Promoting heme synthesis by ALA supplementation may thus represent a promising new anti-cancer strategy, particularly in cancers that are sensitive to altered redox signaling.

In second project, we investigated transcription changes triggered by DNA damage response (DDR). These changes depend on nature of DNA damage, activation of checkpoint kinases, and stage of cell cycle. The transcription changes can be localized and affect only damaged DNA, but they can also be global and affect genes that are not

damaged. While the purpose of localized transcription inhibition is to avoid transcription of damaged genes and to make DNA accessible for repair, purpose and mechanisms of global transcription inhibition of not damaged genes is not well understood. A brief cell treatment with hydroxyurea (HU) globally inhibits RNA synthesis and transcription by RNA polymerase I, II, and III (RNAPI, RNAPII, and RNAPIII). HU triggers RNAPII accumulation at 3' ends of genes, indicating defect in transcriptional termination and pre-mRNA 3' end processing. Interestingly, we observe destabilization of mRNAs after HU treatment. The HU-triggered RNAPII accumulation at 3' ends of genes is exacerbated when checkpoint kinase Mec1p is inactivated, suggesting involvement of DNA damage checkpoint in transcriptional termination.

ACKNOWLEDGEMENTS

This thesis is the cumulation of five years of work at St. John's University. I wish to thank numerous people for contributing to this work. First and foremost, I would like to express my sincere gratitude to my advisor Dr. Ales Vancura for always providing his support in reviewing my progress constantly and guiding me through my PhD studies.

Besides my advisor, I express gratitude towards all my committee members- Dr. Ivana Vancurova, Dr. Yan Zhu, Dr. Matteo Ruggiu, and Dr. Yong Yu for their valuable advice towards this research.

I am extremely thankful to Dr. Ivana Vancurova and Dr. Yan Zhu for always supporting me and giving me an opportunity to work in their lab and learn from them. I would like to thank Dr. Meenhaj Uddin and Dr. Yue Zou for their support and help to start this study in the first place. I would like to thank all the lab members -Shreya Nagar, Madhura Bhagwat, Riddhi Mehta, Bijaya Gaire and Dr. Pengli Bu for their invaluable support, discussions and help throughout these 5 years.

A special thanks to Jasleen, Jagjit, Jaspreet, and Sveta for being with me throughout this journey. Thank you for always putting your faith in me. I wouldn't be where I am today without your support and encouragement.

I would like to express my deepest gratitude to my mother, brother, and family for all their love and support that kept me going through this journey.

TABLE OF CONTENTS

ACKNOWLEDGEMENTS ii

LIST OF TABLES vi

LIST OF FIGURES vii

SECTION I..... 1

Introduction 1

Results 3

 ALA represses oxidative metabolism and glycolysis in ovarian cancer and TNBC
 cells 3

 ALA destabilizes Bach1 in SKOV3 and MDA MB 231 cells and activates AMPK in
 MDA MB 231 cells 5

 AMPK represses oxidative metabolism and glycolysis in both ovarian cancer and
 TNBC cells 6

 Bach1 has a cell type-specific role in regulation of oxidative metabolism 7

 Cells with different activities of aerobic metabolism display unique patterns of ALA
 sensitivity 8

Discussion 9

Materials and Methods 12

 Reagents 12

 Cell culture 12

Transfection with siRNA.....	13
Wound-healing scratch assay	13
Heme assay	14
Lactate assay.....	14
Oxygen consumption rate (OCR) and Extracellular acidification rate (ECAR)	15
Real-time RT-PCR	15
Western blot.....	16
Statistical analysis.....	16
SECTION II	17
Introduction	17
Results	19
HU globally inhibits RNA synthesis	19
Transcriptional effect of HU is attenuated in checkpoint mutants and by altered chromatin structure	21
HU removes RNAPII from chromatin in a gene-specific manner	23
HU triggers RNAPII accumulation at 3' end of genes	24
HU destabilizes mRNAs.....	25
Discussion	28
Materials and Methods	31
Yeast Strains and Media	31

4tU labeling and purification of nascent RNA	31
Slot blot analysis of biotinylated RNA.....	32
Real-time RT-qPCR	33
mRNA decay rates.....	33
ChIP assays.....	34
Statistical analysis.....	34
REFERENCES.....	65

LIST OF TABLES

Table 1 Yeast strains used in this study	35
Table 2 Mammalian Primer sequences for RT-qPCR	37
Table 3 Yeast Primer sequences for RT-qPCR.....	38
Table 4 Primer sequences for ChIP assays	39

LIST OF FIGURES

Figure 1. ALA inhibits mitochondrial respiration and aerobic glycolysis in SKOV3 cells.	41
Figure 2. ALA inhibits mitochondrial respiration and aerobic glycolysis in MDA MB 231 cells.	43
Figure 3. ALA destabilizes Bach1 in SKOV3 and MDA MB 231 cells and activates AMPK in MDA MB 231 cells.....	45
Figure 4. AMPK inhibits mitochondrial respiration and aerobic glycolysis in SKOV3 cells.	46
Figure 5. AMPK inhibits mitochondrial respiration and aerobic glycolysis in MDA MB 231 cells.	48
Figure 6. Bach1 regulates mitochondrial respiration in SKOV3 cells.....	50
Figure 7. Bach1 regulates mitochondrial respiration in MDA MB 231 cells.	52
Figure 8. Cells with different activities of aerobic metabolism display unique patterns of ALA sensitivity.	54
Figure 9. HU globally inhibits RNA synthesis and transcription by RNAPI, II, and III..	55
Figure 10. The transcriptional effect of HU is attenuated in checkpoint and chromatin mutants.....	57
Figure 11. HU removes RNAPII from chromatin in a gene-specific manner.	59

Figure 12. HU triggers RNAPII accumulation in 3' end of genes.....	61
Figure 13. HU destabilizes mRNAs.....	63

SECTION I

Introduction

Cancer cells undergo a complex rearrangement of metabolic pathways involved in biosynthetic processes to support tumor initiation and progression [1]. Altered metabolism has long been considered as a consequence of cell transformation rather than an active participant in tumorigenesis. However, more recent cancer metabolism studies provide many examples of metabolic activities that actively contribute to cell transformation and promote tumorigenesis [1]. One of the hallmarks of cancer is a high rate of glucose uptake and lactate production regardless of oxygen availability, referred to as the “Warburg effect” [2]. The high glycolytic rate supports the biosynthetic needs of proliferating cancer cells by providing intermediates of the glycolytic pathway for anabolic reactions. In addition, many tumor cells overexpress genes encoding metabolic enzymes that facilitate synthesis of ribose 5-phosphate, NADPH, fatty acids, and glycerophospholipids [3-6]. Despite the diversion of carbon flux away from the tricarboxylic acid (TCA) cycle, electron transport chain (ETC), and oxidative phosphorylation (OXPHOS) pathways, most tumors contain functional mitochondria. However, due to the decreased metabolic flux through the TCA cycle in many tumors, intermediates of the TCA cycle can become limiting for synthesis of certain amino acids and cancer cell proliferation [7,8]. Thus, targeting glycolysis, ETC, OXPHOS, and TCA cycle have emerged as a potential therapeutic strategy in some cancers [9-16].

Heme has a potential to regulate glycolysis, ETC, OXPHOS, and TCA cycle [17]. Heme is an essential cofactor of several enzymes of the ETC and is required for ATP production by the mitochondrial ETC and OXPHOS. Increased heme synthesis is

associated with disruption of the Warburg effect and increased ETC and OXPHOS [18-20]. In yeast cells, increased synthesis of heme induces oxidative metabolism [21]. On the other hand, free heme that is not incorporated into hemoproteins catalyzes production of free radicals through Fenton chemistry [22] and elevated synthesis of heme or accumulation of intermediates in heme biosynthetic pathway may trigger increased synthesis of ROS [23]. In addition, cellular heme level regulates the stability of Bach1 (BTB domain and CNC homolog 1). Bach1 is a transcriptional regulator that activates expression of glycolytic genes and represses transcription of the TCA cycle and ETC genes in lung and breast cancer cells [24-26]. In addition, Bach1 activates transcription of genes important for cell migration and promotes metastasis [27-29]. Heme binds to Bach1 and stimulates its degradation [30]. Under normal redox conditions, Bach1 binds to antioxidant response elements (AREs) in the promoters of antioxidant genes, such as heme oxygenase -1 (HO-1), and represses their transcription. Oxidative stress elevates intracellular level of free heme by releasing heme from hemoproteins, leading to degradation of Bach1 and transcriptional induction of antioxidant genes, such as catalase. Stabilization of Bach1 was recently implicated in lung cancer metastasis [24,25]. The level of Bach1 is also elevated in triple-negative breast cancer (TNBC), leading to lower activity of TCA cycle and decreased transcription of ETC genes. Suppressing or destabilizing Bach1 renders TNBC cells sensitive to ETC inhibitors, such as metformin [26].

In this study, we explored the role of cellular heme level in regulation of Warburg effect and expression of pro-metastatic genes in ovarian cancer and TNBC cells. Additional motivation for this study was to determine whether supplementation with

heme precursor 5-aminolevulinic acid (ALA) downregulates Bach1. We show that ALA supplementation leads to downregulation of glycolysis, mitochondrial respiration, as well as cell migration. The underlying mechanisms differ in ovarian and TNBC cells, but likely involve destabilization of Bach1, activation of AMP-activated protein kinase (AMPK), and induction of anti-oxidant response.

Results

ALA represses oxidative metabolism and glycolysis in ovarian cancer and TNBC cells

Since many tumors display the Warburg effect, many anti-cancer strategies aim to disrupt the aerobic glycolysis and promote oxidative phosphorylation. Heme has the potential to regulate glycolysis, TCA cycle, ETC, and OXPHOS. The first and rate-limiting step in heme synthesis is production of ALA [17]. Oral administration of the heme precursor ALA in mouse promotes aerobic energy metabolism in the liver [18]. In addition, ALA disrupts the Warburg effect and increases oxidative phosphorylation in human lung carcinoma cells [19].

To investigate whether stimulation of heme synthesis by ALA supplementation would affect the key metabolic pathways, we first determined heme levels in SKOV3 cells grown in the presence of ALA (Fig. 1A). As expected, addition of the heme precursor ALA to cell culture medium elevated the cellular heme levels. Cell viability was not significantly affected by the used ALA doses; however, cell proliferation was significantly inhibited by ALA (Fig. 1B). The increased heme levels were also reflected in dramatically upregulated heme oxygenase (HO-1) mRNA levels (Fig. 1C).

Transcription of catalase was also increased (Fig. 1D), indicating that the increased

cellular heme level in ALA-supplemented cells triggered increased synthesis of ROS, consistently with the role of free heme in ROS production [22]. ALA supplementation also reduced oxygen consumption rate (OCR) (Fig. 1E) and extracellular acidification rate (ECAR) and lactate accumulation in the medium (Fig. 1F). OCR reflects the activity of the ETC and OXPHOS. ECAR reflects production of lactic acid generated by aerobic glycolysis. ALA reduced basal respiration, as well as maximal respiration, and ATP production. ALA also reduced transcription of glycolytic genes glyceraldehyde-3-phosphate dehydrogenase (GAPDH) and hexokinase 2 (HK2) (Fig. 1F). Despite of suppressing OCR, ALA supplementation elevated transcription of several ETC and OXPHOS genes (Fig. 1G). In agreement with the role of Bach1 as a transcriptional activator of metastatic genes and a driver of cell migration [27-29], the expression of genes involved in metastasis and cell migration (MMP1, MMP9, MMP13, CXCR4, and vimentin), as well as cell migration, were reduced (Fig. 1H and I).

Similarly to SKOV3 cells, ALA supplementation of TNBC cells MDA MB 231 also elevated heme levels (Fig. 2A) without affecting cell viability. Cell proliferation was inhibited only at 10 mM concentration of ALA (Fig. 2B). In comparison with SKOV3 cells, proliferation of MDA MB 231 cells was significantly less affected by ALA (compare Fig. 1B and 2 B). Elevated heme levels due to ALA supplementation significantly induced HO-1 transcription (Fig. 2C) and slightly induced expression of catalase (Fig. 2D). Again, similarly to SKOV3 cells, ALA supplementation of MDA MB 231 cells reduced OCR (Fig. 2E) and ECAR and lactate accumulation in the medium (Fig. 2F) and increased transcription of several ETC and OXPHOS genes (Fig. 2G), while the mRNA levels of GAPDH and HK2 were not significantly affected (Fig. 2F).

However, in comparison with SKOV3 cells, MDA MB 231 cells had more active glycolysis (compare Fig. 1F and 2F). Despite elevating transcription of MMP1, MMP9, and MMP13 (Fig. 2H), ALA supplementation slightly reduced cell migration (Fig. 2I).

ALA destabilizes Bach1 in SKOV3 and MDA MB 231 cells and activates AMPK in MDA MB 231 cells

Binding of heme to Bach1 inhibits its DNA binding activity and induces its nuclear export, resulting in polyubiquitination and degradation of Bach1 [30]. Consistently with the elevated heme levels, ALA supplementation reduced the Bach1 levels in both SKOV3 and MDA MB 231 cells (Fig. 3A and B). Since supplementation with ALA reduced OCR and ECAR in both SKOV3 and MDA MB 231 cells, indicating downregulation of glycolysis and ETC/OXPHOS, two main energy-producing pathways, we determined the activation status of AMP-activated protein kinase (AMPK), an energy sensor and master regulator of metabolism. Activation of AMPK is associated with increased AMPK phosphorylation at Thr¹⁷², a hallmark of AMPK activation by liver kinase B (LKB1) [36]. Another hallmark of AMPK activation is phosphorylation of acetyl-CoA carboxylase (ACC) at Ser⁷⁹ [37]. Notwithstanding repression of both glycolysis and oxidative metabolism, supplementation with ALA did not result in increased phosphorylation of AMPK (pAMPK) or ACC (pACC) in SKOV3 cells (Fig. 3C). However, ALA induced activation of AMPK in MDA MB 231 cells, as judged from increased phosphorylation of AMPK and ACC (Fig. 3D). This is quite surprising, given that the proliferation of SKOV3 cells was significantly more affected by ALA than proliferation of MDA MB 231 cells.

AMPK represses oxidative metabolism and glycolysis in both ovarian cancer and TNBC cells

Despite repressing both glycolysis and oxidative metabolism, promoting heme synthesis by ALA supplementation did not activate AMPK in SKOV3 cells. However, treating SKOV3 cells with AMP homolog 5-amino-1- β -D-ribofuranosyl-1*H*-imidazole-4-carboxamide (AICAR) activated AMPK, as evidenced by increased levels of both pAMPK and pACC (Fig. 4A). We conclude that AMPK in SKOV3 cells is competent for activation; however, SKOV3 cells likely have metabolic plasticity that allows them to adjust their metabolism to avoid the energy deprivation due to ALA treatment. As expected, treatment of SKOV3 cells with AICAR did not elevate cellular heme levels (Fig. 4B). Interestingly, AICAR treatment paralleled the effects of ALA supplementation in both SKOV3 and MDA MB 231 cells and induced HO-1 and catalase transcription, albeit to a lesser degree than ALA supplementation (Fig. 4C). AICAR treatment also reduced OCR (Fig. 4D), ECAR and lactate accumulation in the medium (Fig. 4E), as well as transcription of several metastatic genes (Fig. 4F) and cell migration (Fig. 4G). Similarly to SKOV3 cells, AICAR treatment of MDA MB 231 cells activated AMPK (Fig. 5A) and did not elevate cellular heme levels (Fig. 5B), but slightly induced HO-1 and catalase transcription (Fig. 5C). AICAR treatment also reduced OCR (Fig. 5D), ECAR and lactate accumulation in the medium (Fig. 5E), as well as transcription of several metastatic genes and cell migration (Fig. 5F and G). These results suggest that at least in MDA MB 231 cells, where AMPK is activated by ALA supplementation, AICAR treatment resulting in AMPK activation may contribute to the inhibitory effects of ALA on glycolysis, aerobic metabolism, and cell migration.

Bach1 has a cell type-specific role in regulation of oxidative metabolism

Since increased levels of cellular heme by ALA supplementation reduced Bach1 protein levels, we wanted to determine whether Bach1 contributes to the regulation of glycolysis, aerobic metabolism, and cell migration. As shown in Fig. 6A, small interfering RNA (siRNA)-mediated silencing of Bach1 suppressed the Bach1 mRNA and protein levels in SKOV3 cells by about 75%. Consistently with the role of Bach1 as a suppressor of HO-1, Bach1 silencing significantly elevated the HO-1 transcription (Fig. 6B). Contrary to our expectation, however, Bach1 silencing reduced the OCR (Fig. 6C), as well as mRNA levels of ETC genes *NDUFB5* and *COX17* (Fig. 6D). In agreement with the role of Bach1 in transcription of metastatic genes, silencing of Bach1 reduced transcription of *MMP9* and *CXCR4*, genes involved in metastasis and cell migration (Fig. 6F). However, Bach1 silencing did not significantly affect migration of SKOV3 cells measured by the scratch assay (Fig. 6G).

Bach1 silencing in TNBC cells MDA MB 231 significantly suppressed Bach1 protein and mRNA levels (Fig. 7A) and induced expression of HO-1 (Fig. 7B). Unlike in SKOV3 cells, Bach1 silencing in MDA MB 231 cells elevated OCR (Fig. 7C). This is in agreement with the role of Bach1 in suppression of ETC genes in TNBC cells [26], but contrary to the role of Bach1 in regulation of oxidative metabolism in SKOV3 cells (Fig. 6C). These findings suggest that the role of Bach1 in regulation of OCR is cell specific. Bach1 silencing in MDA MB 231 cells elevated mRNA level of only one of the several ETC genes examined (*ATP5D*; Fig. 7D). Bach1 silencing in MDA MB 231 cells also slightly elevated ECAR (Fig. 7E). Contrary to the role of Bach1 as an activator of transcription of metastatic genes, silencing of Bach1 did not affect mRNA levels of

MMP9, CXCR4, and vimentin, and elevated transcription of only MMP1 and MMP13 (Fig. 7F).

Cells with different activities of aerobic metabolism display unique patterns of ALA sensitivity

In comparison with SKOV3 cells, MDA MB 231 cells displayed slightly higher activity of aerobic metabolism (compare Fig. 1E and 2E) and their proliferation was significantly less affected by ALA treatment (compare Fig. 1B and 2B). To evaluate whether the activity of oxidative metabolism correlates with ALA sensitivity, we compared the OCR and proliferation in several cell lines with different activities of oxidative metabolism (Fig. 8). Breast cancer MCF7 cells and lung cancer H1299 cells displayed very high OCR and their proliferation was not significantly affected by 0.1 mM and 1 mM ALA concentrations. However, their proliferation was completely inhibited by 10 mM ALA. Despite having lower OCR than MCF7 and H1299 cells, proliferation of prostate cancer PC3 cells at different ALA concentrations displayed similar pattern and was only slightly affected at 0.1 mM and 1 mM ALA; however, at 10 mM, the proliferation of PC3 cells was almost completely inhibited (Fig. 8). In contrast to MCF7 and H1299 cells, MDA MB 468 cells displayed lower OCR and their proliferation was affected by all ALA concentrations. Remarkably, MDA MB 468 cells were able to proliferate even in the presence of 10 mM ALA and the OCR values and the proliferation pattern of MDA MB 468 cells resembles that of MDA MB 231 cells. The ovarian cancer OVCAR3 cells behaved similarly as SKOV3 cells (compare Fig. 1B and 1E with Fig. 8) and displayed the lowest OCR. Similarly to MDA MB 468 cells, their proliferation was

affected by all ALA concentrations and OVCAR3 cells were able to proliferate even in the presence of 10 mM ALA.

Discussion

The key finding of this study is that promoting heme synthesis through ALA supplementation in both ovarian cancer and TNBC cells leads to downregulation of glycolysis, mitochondrial respiration, as well as cell proliferation. In comparison with MDA MB 231 cells, SKOV3 cells displayed lower activities of both glycolytic and aerobic metabolism (compare Fig. 1E and G with 2E and G) and their proliferation was significantly more suppressed by ALA treatment, especially at low ALA concentrations (compare Fig. 1B and 2B). The underlying mechanisms involve destabilization of Bach1, AMPK activation, and inducing anti-oxidant response. This result suggests that cells that rely more heavily on aerobic metabolism for energy production are less sensitive to ALA. To test this notion, we evaluated response to ALA in several cell lines with different activities of oxidative metabolism (Fig. 8). The general conclusion of these studies is that proliferation of cells with a high activity of oxidative metabolism, such as H1299 and MCF7, is not affected by low concentrations of ALA (0.1 and 1 mM), but significantly inhibited at high ALA concentration (10 mM). In contrast, proliferation of cells with a lower activity of oxidative metabolism, such as MDA MB 468 and OVCAR3, is affected even by low (0.1 and 1 mM) ALA concentrations. The inverse correlation between the OCR and ALA sensitivity is particularly interesting for cells with the same origin, as shown for MCF7, MDA MB 231, and MDA MB 468 (Fig. 2 and 8). Moreover, SKOV3

and OVCAR3 cells have lower OCR and are more sensitive to ALA than MDA MB 231, and MDA MB 468 cells (Fig. 1, 2, 8).

Heme serves as a prosthetic group in proteins that sense, transport, or use oxygen, such as hemoglobin, myoglobin, cytochrome complexes, catalases, and cyclooxygenases. Heme is also required for ATP production by the mitochondrial ETC and OXPHOS and controls activities of a number of proteins involved in regulation of metabolism and transcription [17]. One of heme's cellular targets is Bach1. Bach1 is a transcriptional regulator that controls expression of several groups of genes important for metabolism and metastasis of cancer cells. In lung cancer, administration of antioxidants N-acetylcysteine or vitamin E reduces level of free heme, which stabilizes Bach1. Bach1, in turn, activates HK2 and GAPDH and stimulates glycolysis-dependent metastasis [24]. About 30% of non-small-cell lung cancers display increased expression of antioxidant genes due to acquiring mutations that stabilize Nrf2, a transcription factor that regulates expression of antioxidant genes. The elevated activity of Nrf2 leads to increased expression of HO-1 and degradation of heme, resulting in stabilization of Bach1 and increased transcription of pro-metastatic genes [25]. The level of Bach1 is also elevated in triple-negative breast cancer (TNBC), leading to lower activity of TCA cycle and decreased transcription of ETC genes. Suppressing or destabilizing Bach1 renders TNBC cells sensitive to ETC inhibitors, such as metformin [26]. These reports highlight that Bach1 targeting is a possible strategy for cancer treatment.

Activating heme synthesis by exogenous administration of ALA provides an effective way to regulate Bach1 stability (Fig. 3A and B). In SKOV3 cells, ALA supplementation paralleled the effects of Bach1 silencing (Fig. 6) and reduced ETC and

OXPPOS (Fig.1). These results indicate that Bach1 is a positive regulator of ETC and OXPPOS in SKOV3 cells and likely mediates the effect of increased level of heme on aerobic metabolism. In MDA MB 231 cells, ALA supplementation reduced ETC, OXPPOS, and glycolysis (Fig.2). However, Bach1 silencing had the opposite effect and activated aerobic metabolism (Fig. 7). We conclude that the effect of elevated level of heme on ETC, OXPPOS, and glycolysis in MDA MB 231 cells (Fig. 2) is at least partly mediated by the activation of AMPK elicited by ALA supplementation (Fig. 3D and Fig. 5). The opposite effects of Bach1 silencing on aerobic metabolism in SKOV3 and MDA MB 231 cells (Fig. 6 and 7) suggest that the role of Bach1 in regulation of oxidative metabolism depends on the context and is rather cell-type specific. To determine to what extent the regulation of aerobic metabolism by ALA supplementation is dependent or independent of Bach1 will require *in vitro and in vivo* studies utilizing Bach1 mutants that are not regulated by heme [26, 38].

As indicated by the increased expression of anti-ROS gene catalase in both SKOV3 and MDA MB 231 cells (Fig. 1 and 2), elevated heme levels due to ALA supplementation lead to increased production of ROS [22, 39] and may contribute to the suppression of oxidative metabolism in both cell lines (Fig. 1 and 2). ALA treatment of human hepatocarcinoma cells induced ROS production and inhibited mitochondrial respiration [23]. Modulation of heme synthesis by exogenous administration of ALA is used in photodynamic therapy (PDT) of cancer. ALA induces elevated levels of protoporphyrin IX (PPIX), the ultimate precursor in the heme biosynthetic pathway [40], primarily in cancer cells. PPIX is an efficient photosensitizer and activation of PPIX by light generates ROS in cancer cells, leading to apoptotic cell death [41-43]. The role of

oxidative stress and ROS in tumorigenesis is controversial and many results support the role of ROS in promoting or suppressing tumorigenesis [44-46]. Thus, while our results show that targeting Bach1 by exogenous administration of ALA is quite effective in reducing Bach1 levels, the additional effects of ALA likely involve elevated ROS production. Promoting heme synthesis by ALA supplementation may thus represent a promising new anti-cancer strategy, particularly in cancers that are sensitive to altered redox signaling, or in combination with strategies that target the antioxidant systems or metabolic weaknesses of cancer cells.

Materials and Methods

Reagents

5-Aminolevulinic acid hydrochloride (ALA, A3785) was purchased from Sigma. 5-Amino-1- β -D-ribofuranosyl-1H-imidazole-4-carboxamide (AICAR, 10010241) was purchased from Cayman.

Cell culture

All cell lines were obtained from American Type Culture Collection (ATCC, Manassas, VA, USA). MCF7, H1299 and MDA-MB-231 cells were cultured in Dulbecco's modified Eagle's medium (DMEM) supplemented with 10% heat inactivated fetal bovine serum (FBS; Invitrogen, Grand Island, NY, USA) and antibiotics (100 units/mL penicillin and 100 μ g/ml streptomycin). MDA-MB-468 and SKOV3 cells were cultured in RPMI 1640 medium (Invitrogen) supplemented with 2 mM L-glutamine, 10 mM HEPES, 1 mM sodium pyruvate, 10% heat inactivated

FBS, and antibiotics (100 units/ml penicillin and 100 µg/ml streptomycin). OVCAR3 cells were cultured in RPMI 1640 medium (Invitrogen) supplemented with 2 mM L-glutamine, 10 mM HEPES, 1 mM sodium pyruvate, 20% heat inactivated FBS, and antibiotics (100 units/ml penicillin and 100 µg/ml streptomycin). Cells were seeded (5×10^5 cells/ml) for 24 h in 6-well plates, grown at 37°C with 5% CO₂, and incubated with ALA or AICAR for 24 h. Cell viability was measured using TrypanBlue exclusion. Cell proliferation was measured by CellTiter96 One Solution Cell Proliferation Assay (Promega, Madison, WI) as described [31].

Transfection with siRNA

Human Bach1 (sc-37064), and non-silencing (sc-37007) small interfering RNAs (siRNAs) were obtained from Santa Cruz Biotechnology. Prior to transfection, cells were seeded (2×10^5 cells/ml) into a 6-well plate and incubated in a humidified 5% CO₂ atmosphere at 37°C in antibiotic free medium supplement with 10% FBS for 24 h to about 80% confluence. For each transfection, 80 pmol of either non-silencing siRNA control or Bach1 siRNA were used; cells were transfected 7 h in siRNA transfection medium with siRNA transfection reagent according to manufacturer's instructions (Santa Cruz Biotechnology). After transfection, fresh medium with antibiotics was added, and cells were grown for 24 h.

Wound-healing scratch assay

Cells were seeded in 6-well plates at a density of 5×10^5 cells/ml in medium containing 5% FBS. Once the cells became confluent, a wound area was created by

scraping the cell monolayer with a sterile 200 μ l pipette tip. After washing twice with PBS, DMEM medium without FBS or RPMI 1640 medium without FBS was added to the wells with MDA MB 231 or SKOV3 cells, respectively. The scratch area was monitored under a phase-contrast microscope at 0, 24, 48 and 72 h after transfection. The wound width was measured in five random fields using ImageJ software as described [32] and the average wound width at 72 h was normalized to the average wound width at 0 h.

Heme assay

The amount of heme was measured using heme assay kit (K672-100, BioVision) according to the manufacturer's instruction. Cells were seeded into 6-well plates at a density of 5×10^5 cells/ml in culture medium. After overnight incubation, cells were treated with ALA and AICAR and incubated for 24 h at 37°C in humidified air with 5% CO₂. After 24 h treatment, cells were harvested, washed twice with PBS, and lysed in 50 μ l of 1% NaOH and 5% Triton. Cell lysates were neutralized to pH 7.5 and used to measure the amount of heme.

Lactate assay

Lactate concentration in the culture medium was measured using lactate assay kit (MAK065, Millipore-Sigma) according to the manufacturer's instruction. Cells were seeded into 6-well plates at a density of 5×10^5 cells/ml in culture medium. After overnight incubation, cells were treated with ALA or AICAR, and

incubated for 24 h at 37°C in humidified air with 5% CO₂. After 24 h treatment, cell medium was used to measure lactate concentration.

Oxygen consumption rate (OCR) and Extracellular acidification rate (ECAR)

OCR and ECAR were measured using Seahorse XFp analyzer as described previously [33]. Cells were plated in Seahorse XFp cell culture plates (103022, Agilent) at 20,000 cells/well and incubated overnight. After incubation, cells were treated with ALA and AICAR for 24 h. Cells were washed and incubated with assay medium at 37°C for 1 h in a non-CO₂ incubator. OCR and ECAR were measured using Seahorse XFp mito stress kit (103010, Agilent). OCR was measured under basal conditions followed by the sequential addition of oligomycin (1.5 μM), FCCP (0.5 μM), and rotenone & antimycin A (Rot/AA; 0.5 μM). Derived respiratory parameters are basal respiration (B), proton leak (PL), maximal respiration (MR), non-mitochondrial respiration (NMR), and ATP production (ATPP). For Bach1 suppressed cells, Bach1 siRNA transfection was done as described above. After transfection, cells were seeded in Seahorse XFp cell culture plates and assay were performed as described above.

Real-time RT-PCR

Total RNA was isolated using RNeasy mini-kit (Qiagen, Valencia, CA). The iScript one-step RT-PCR kit with SYBR Green (Bio-Rad) was used as a supermix and 20 ng/μl of RNA was used as template on a Bio-Rad MyIQ Single Color Real-time PCR Detection System (Bio-Rad). The primers used for mRNA quantification are listed in Table I. The results were normalized to 18S ribosomal RNA and the mRNA values were

expressed as a percentage of control or untreated samples, which were arbitrarily set as 100%.

Western blot

Whole cell extracts were prepared and western blotting was performed as described previously [34, 35]. The following primary antibodies were used: anti AMPK monoclonal antibody (2603; Cell Signaling) at a dilution of 1:1000; anti phospho-AMPK (Thr172) monoclonal antibody (pAMPK; 2535; Cell Signaling) at a dilution of 1:1000; anti-acetyl-CoA carboxylase monoclonal antibody (ACCA; 3676; Cell Signaling) at a dilution of 1:1000; anti-phospho acetyl-CoA carboxylase (Ser79) polyclonal antibody (pACCA; 3661; Cell Signaling) at a dilution of 1:1000; anti-Bach1 monoclonal antibody (Bach1; sc-271211; Santa Cruz Biotechnology) at a dilution of 1:1000; anti-actin polyclonal antibody (A5060, Sigma) at a dilution of 1:2000.

Statistical analysis

The results represent at least three independent experiments. Numerical results are presented as means \pm SD. Data were analyzed by using an InStat software package (GrapPAD, San Diego, CA, USA). Statistical significance was evaluated by one-way Anova analysis, and $p < 0.05$ was considered significant.

SECTION II

Introduction

Both exogenous and endogenous factors can generate genotoxic stress and damage cellular DNA [47-49]. Because maintenance of genome stability is crucial for survival, cells have evolved a set of highly conserved mechanisms to sense and signal damaged DNA; these mechanisms are collectively referred to as the DNA damage response (DDR) [49-51]. Major part of DDR is coordinated by DNA damage checkpoint (DDC) [48]. In addition to DDC, eukaryotic cells have DNA replication checkpoint (DRC) that is distinct from the DDC and signals specifically slowly progressing or arrested replication forks [48, 52, 53]. DDC/DRC trigger stalling or arrest of the cell cycle, initiation of DNA repair, and altered regulation of transcription, translation, and the ubiquitin-proteasome system.

The transcriptional changes elicited by genotoxic or replication stress involve RNA polymerase I, II, and III (RNAPI, RNAPII, RNAPIII) [54-60] and depend on the nature of DNA damage, stage of cell cycle, and DDC/DRC activation. Double-stranded DNA (dsDNA) breaks induce mostly localized inhibition of transcription around the dsDNA breaks [61]. Base damage appears to cause temporary pausing of elongating RNAPII [62]. In contrast, bulky DNA lesions caused by chemical modifications or UV irradiation elicit RNAPII stalling or arrest, leading to transcription-coupled nucleotide excision repair (TC-NER). If TC-NER is unsuccessful, Rpb1p, the largest subunit of RNAPII, is ubiquitinated and degraded as a “mechanism of last resort” [63]. In addition, DRC regulates transcription during the S phase, when replication and transcription machineries compete for the same DNA template and can therefore interfere with each

other and cause DNA damage. DRC temporarily downregulates transcription by RNAPII and RNAPIII during encounters of transcription and replication machineries. DRC activation during replication stress triggers disassembly of the preinitiation complexes at tRNA genes [64] and removes RNA polymerases from chromatin [65, 66]. Genotoxic stress does not trigger transcriptional changes only in the vicinity of DNA damage. DDC/DRC activation regulates transcription of specific groups of co-regulated genes by phosphorylating transcription factors, independently on where in the genome the site(s) of DNA damage are located [67-72].

Interesting and incompletely understood aspect of transcriptional response to genotoxic stress is global inhibition of transcription that affects also expression of genes encoded by DNA that was not damaged by genotoxic stress [55, 57, and 58]. The immediate transcriptional response to UV exposure is global inhibition of transcription elongation [73, 74], followed by inhibition of transcription initiation [74-76]. An important event in response to genotoxic stress and genome-wide transcription shutdown is regulation of Rpb1p subunit of RNAPII by ubiquitination at K₁₂₆₈ (K₁₂₄₆ in yeast) and degradation [63]. However, it is not known whether this is the only mechanism of global inhibition of transcription after genotoxic stress.

The likely purpose of the global inhibition of transcription by RNAPI, RNAPII, and RNAPIII is to make DNA accessible for repair, avoid transcription of damaged genes, and conserve cellular resources; however, the mechanisms are largely unknown. Our results show that a relatively brief treatment with HU globally inhibits RNA synthesis and transcription by RNAPI, RNAPII, and RNAPIII. HU triggers RNAPII accumulation at the 3' ends of protein coding sequences (CDS) and 3'-untranslated

regions (3'-UTR), indicating defect in transcriptional termination and pre-mRNA 3' end processing. Interestingly, we observed destabilization of several mRNAs after HU treatment. The HU-triggered RNAPII accumulation at the 3' ends of CDS and 3'-UTR is exacerbated in *mec1Δsm11Δ* cells, suggesting that Mec1p is involved in transcriptional termination.

Results

HU globally inhibits RNA synthesis

HU is an inhibitor of ribonucleotide reductase, decreases dNTP levels and slows down progression of replication forks, resulting in activation of DRC. HU does not directly damage DNA; however, stalled replication forks occasionally collapse or break, causing secondary DNA damage. Since yeast can grow in the presence of 200 mM HU, it is likely that a 30 min HU treatment does not cause extensive DNA damage and the transcriptional responses to HU are due to activation of checkpoint kinases of DRC [77, 78].

To determine whether treatment with HU globally inhibits RNA synthesis, cells were grown in rich YPD medium, treated with 200 mM HU for 30 min, and subsequently pulse labeled with 4-thiouracil (4tU). *In vivo* pulse labeling of RNA with 4tU for a short period of time and quantification of the labeled RNA provides a convenient readout of transcriptional rate. Total RNA was isolated, labeled with biotin, and analyzed by slot blot analysis with streptavidin-horseradish peroxidase detection. The results indicate that treatment with HU reduced total RNA synthesis by about 30% (Fig. 9A).

Since HU inhibits transcription of ribosomal RNA by RNAPI [59], we wanted to determine whether HU also affects RNA synthesis by RNAPII and RNAPIII. For this analysis, cells were pulse-labeled with 4tU and mixed in a fixed ratio with labeled *S. pombe* cells for normalization. RNA was isolated, biotinylated, and nascent RNA was isolated on streptavidin-coated magnetic beads. The RNAPII transcripts of *PYK1*, *RPL3*, *YEF3*, *PMAI*, and *ADH1*, and RNAPIII transcripts of *SCR1*, *SNR6*, 5S RNA, *SNR52*, *RPR1*, and *SUP4* in the nascent RNA were quantified by reverse transcription-quantitative PCR (RT-qPCR) (Fig. 9B). All examined transcripts were reduced by the HU treatment to levels ranging from about 60% for *PYK1* to less than 10% for *PMAI* in comparison with the untreated samples (Fig. 9B).

To determine whether HU treatment affects the assembly of the preinitiation complexes (PICs) for RNAPI, RNAPII, and RNAPIII, we determined the occupancy of Spt15p, the yeast TATA-binding protein, to the promoters of genes transcribed by RNAPI, II, III (Fig. 9C). In addition, we determined the occupancy of Rpa190p, the largest subunit of RNAPI, over the ribosomal RNA gene *RDN37*, occupancy of Rpb1p, the largest subunit of RNAPII, in the promoter regions of several genes transcribed by RNAPII, and occupancy of Ret1p, the second largest subunit of RNAPIII, over several genes transcribed by RNAPIII (Fig. 9D). The results reveal that HU does not uniformly inhibit assembly of PICs at RNAPI, RNAPII, and RNAPIII promoters. While the occupancies of Spt15p in the promoters of RNAPI-transcribed *RDN37* and RNAPIII-transcribed 5S ribosomal RNA genes were not affected by HU, the occupancies of Spt15p at all examined RNAPII promoters and the remaining RNAPIII promoters were reduced by HU (Fig. 9C). The occupancy of Rpa190p was significantly reduced throughout the

ribosomal RNA gene coding region. The occupancies of Rpb1p in the promoter-proximal regions of CDS of RNAPII genes were reduced, but to different levels. HU caused a significant reduction of Rpb1p occupancy in all tested genes except *EDC1* and *ACT1*. Except for *SNR6* and *RPRI*, the Ret1p occupancy was not reduced at any of the examined RNAPIII genes (Fig. 9D).

Transcriptional effect of HU is attenuated in checkpoint mutants and by altered chromatin structure

The effect of HU on transcription would be expected to require the checkpoint kinases and occur during the S phase. To test this prediction, we calculated fractions of *PYK1*, *RPL3*, and *YEF3* remaining after 30 min of HU exposure in wild-type (WT) cells and cells with inactivated checkpoint kinases *mec1Δsml1Δ*, *tel1Δ*, *rad53Δsml1Δ*, *chk1Δ*, and *dun1Δ* cells; *mec1Δ* and *rad53Δ* cells are viable only if harboring the *sml1Δ* mutation [79]. In WT cells, the level of repression varied from about 50 % for *PYK1*, to about 10 % for *RPL3* (Fig. 10A). The HU-mediated repression was most significantly attenuated in *mec1Δsml1Δ*, *rad53Δsml1Δ*, and *mrc1Δ* cells. This result is consistent with the notion that the effect of HU on transcription requires activation of DRC.

The extent of the HU-mediated transcriptional repression differed significantly amongst individual genes, with *PYK1* being relatively immune to transcriptional repression and *RPL3* and *YEF3* being significantly more responsive. This can be at least partly explained by the differences in the stabilities of the corresponding mRNA. *PYK1* mRNA is significantly more stable than *RPL3* or *YEF3* mRNAs [80]. In general, steady-

state levels of mRNAs with greater stability, such as *PYK1*, would be expected to be affected less by 30 min of HU-mediated transcriptional repression.

The HU-mediated repression of histone genes is attenuated in strains with deletions of histone chaperones [81]. To find out if histone chaperones or other factors required for chromatin assembly and architecture are required for HU-mediated transcriptional repression, we determined *PYK1*, *RPL3*, and *YEF3* mRNA levels in WT, *asf1Δ*, *rtt106Δ*, *cac1Δ*, *hir1Δ*, *spt10Δ*, and *spt21Δ* cells before and after 30 min exposure to HU. While *ASF1*, *RTT106*, *CAC1*, and *HIR1* encode histone chaperones, *SPT10* and *SPT21* encode transcription factors specific for histone genes. The results showed that the HU-mediated transcriptional repression was attenuated by all of the tested chromatin factors (Fig. 10B). The easiest interpretation of this result is that the altered chromatin structure in these mutants permits transcription in the presence of HU. However, this interpretation is complicated by the fact that variety of factors, including histone chaperones, are required for suppression of transcriptional initiation from within coding regions [82-86]. Thus, this cryptic transcription may be at least partly responsible for the suppression of the HU-mediated transcriptional repression in mutants with altered chromatin structure.

The steady-state level of RNA is determined by its synthesis and degradation rates. To assess the effect of HU on transcription rate, we measured nascent RNA in WT and *mec1Δsml1Δ* cells before and after HU treatment (Fig. 10C). The results were in agreement with the measurements of total RNA and showed attenuated HU-mediated transcriptional repression in *mec1Δsml1Δ* cells in comparison with WT cells not only for

RNAPII transcripts *PYK1*, *RPL3*, *YEF3*, and *PMA1*, but also for RNAPIII transcripts *SCR1*, *SNR6*, *5S RNA*, *RPR1*, and *SUP4* (Fig. 10C).

Since the DRC is activated during the S phase, we compared the extent of the HU-mediated transcriptional suppression in WT cells arrested in G1 phase with WT cells released into S phase (Fig. 10D). The results showed that cells in G1 phase are significantly less responsive to transcription repression by HU than S phase cells.

HU removes RNAPII from chromatin in a gene-specific manner

Our results showed that HU reduces occupancy of Rpb1p, the largest subunit of RNAPII, in the promoter-proximal regions of CDS (Fig. 9D). To determine whether HU-mediated RNAPII eviction from chromatin occurs evenly throughout CDS, we determined Rpb1p occupancies within the promoters and coding regions of *PYK1*, *RPL3*, *YEF3*, *PMA1*, *ADH1*, and *YLR454* genes in WT and *mec1Δsm11Δ* cells before and after treatment with HU (Fig. 11). Comparison of the profiles allows several conclusions. First, HU does not significantly affect processivity of RNAPII. Second, the Rpb1p occupancies in WT and *mec1Δsm11Δ* cells before HU treatment did not significantly differ in any of the tested genes. Third, and rather surprisingly, HU significantly decreased the Rpb1p occupancies throughout the CDS of only *RPL3* and *YEF3* genes, while the Rpb1p occupancies within the CDS of *PYK1*, *PMA1*, *ADH1*, and *YLR454* genes in WT cells were not significantly reduced. (Fig. 11). This finding contrasts with significantly reduced nascent mRNA levels of all three genes after HU treatment (Fig. 9B). Fourth, in many positions throughout the CDS of *PMA1*, *YEF3*, *RPL3*, and *YLR454* genes, the

Rpb1p occupancy after the HU treatment was higher in *mec1Δsml1Δ* cells than in WT cells, particularly in the 3' portions of the CDS and 3'-UTR.

HU triggers RNAPII accumulation at 3' end of genes

The observation that Rpb1p occupancy after the HU treatment was higher at the 3' portions of the CDS and 3'UTR in *mec1Δsml1Δ* cells than in WT cells can be explained by at least two mutually non-exclusive mechanisms. The first possibility is that HU triggers cryptic transcription, and this effect is exacerbated in *mec1Δsml1Δ* cells. The second possibility is that HU treatment causes defect in transcriptional termination and perhaps RNAPII stalling within the 3' portions of CDS and 3'-UTR, particularly in *mec1Δsml1Δ* cells. One of the hallmarks of cryptic transcription is elevated Rpb1p occupancy at the 3' ends of CDS in comparison with 5' ends. To test whether treatment with HU leads to inappropriate transcriptional initiation within coding regions, we evaluated the ratios of Rpb1p occupancies at the 3' and 5' ends of the CDS in *PYK1*, *RPL3*, *YEF3*, *PMA1*, *ADHI*, and *YLR454* genes in WT and *mec1Δsml1Δ* cells before and after treatment with HU. The 3'/5' ratios of Rpb1p occupancies do not significantly differ between WT and *mec1Δsml1Δ* cells (Fig. 12A). Except for *YLR454*, HU treatment of WT cells elevated the Rpb1p 3'/5' ratios for other tested genes. In *mec1Δsml1Δ* cells, HU treatment caused dramatic increase in the Rpb1p 3'/5' ratios for all tested genes (Fig. 12A).

To test whether the elevated Rpb1p 3'/5' ratios observed in WT and *mec1Δsml1Δ* cells after HU treatment really reflect inappropriate transcriptional initiation within coding regions, we determined mRNA levels in wild-type and *mec1Δsml1Δ* strains at the

5' and 3' portions of CDS of *PYK1*, *RPL3*, *YEF3*, *PMA1*, *ADHI*, and *YLR454* genes (Fig. 12B). As a positive control, we included *asf1* Δ strain, known to exhibit cryptic transcription and elevated 3'/5' mRNA ratios of number of genes, including *FLO8* and *VPS72* (82-87). To make the mRNA levels at the 5' and 3' end of each gene comparable, we corrected the results for the efficiency of primers. As expected, the 3'/5' mRNA ratios of *FLO8* and *VPS72* genes were elevated in *asf1* Δ strain and these ratios were not exacerbated by the HU treatment (Fig. 12B). Except for *YLR454* gene, expressed from a strong inducible *GALI* promoter, treatment of wild-type cells with HU did not elevate the 3'/5' mRNA ratios of the other examined genes. Since the Rpb1p occupancy within the *YLR454* gene was higher than in the other tested genes (Fig. 11), we conclude that in WT cells, HU may trigger cryptic transcription only in very highly transcribed genes. Surprisingly, we detected cryptic transcription of *YLR454* gene in untreated as well as treated *mecl1* Δ *sm11* Δ cells (Fig. 12B). This finding indicates that Mec1p may have a novel role in suppressing cryptic transcription of highly transcribed genes. Since suppression of cryptic transcription within genes requires normal histone levels and function of number of chromatin regulators [86], this result suggests that the treatment with HU employed here did not result in gross chromatin changes that would lead to widespread cryptic transcription.

HU destabilizes mRNAs

We were surprised by the finding that the Rpb1p occupancies in the promoter and entire CDS of *PMA1*, *PYK1*, and *ADHI* in WT cells are not significantly reduced by HU (Fig. 11), despite a significant decrease in the nascent mRNA levels (Fig. 9B). These

results suggest that HU does not affect the number of RNAPII molecules transcribing *PMA1*, *PYK1* and *ADHI* genes, but affects the production of the corresponding mRNAs. The simplest possible explanation would be that HU reduces the rate of transcriptional elongation or perhaps induces irreversible stalling of RNAPII on the DNA template. To test this scenario, we employed the very long *YLR454* gene (8 kb) under the control of galactose-inducible *GALI* promoter [88]. This reporter construct allows measurements of transcription elongation rate by monitoring Rpb1p occupancies at regularly spaced positions on *YLR454* gene at different time points during the “last wave of transcription” after promoter shut down by glucose. These experiments showed that HU does not reduce the rate of transcriptional elongation (Fig. 13A). The results also show that HU does not cause irreversible stalling of RNAPII, since the RNAPII within the coding region of *YLR454* is able to finish the transcription cycle and completely clear the gene after the promoter shut down by glucose.

Another mechanism to reconcile the difference in the effect of HU on mRNA synthesis and RNAPII occupancy on *PMA1*, *PYK1*, and *ADHI* genes would be degradation of the produced mRNAs. To assess the involvement of the two major 5' to 3' exonucleases Rat1p and Xrn1p in HU-mediated repression of mRNA synthesis, we calculated fractions of *PYK1*, *RPL3*, *YEF3*, *PMA1*, and *ADHI* mRNAs remaining after 30 min of HU exposure in *xrn1Δ* cells and *rat1-1^{ts}* cells grown at 30°C and exposed for 1 h to 37°C, restrictive temperature for *rat1-1^{ts}* cells (Fig. 13B). The HU-mediated repression was significantly attenuated in *rat1-1* cells at 30°C as well as 37°C, and in *xrn1Δ* cells. This result suggests that at least part of the repressive effect of HU on mRNA levels is mediated by mRNA degradation.

To test directly, whether HU treatment affects mRNA stability, we determined half-lives of *PYK1*, *RPL3*, *YEF3*, *PMA1*, and *ADH1* mRNAs in WT and *mec1Δsm11Δ* cells before and after HU treatment (Fig. 13C). Transcription was inhibited by thiolutin and mRNA levels were followed by RT-qPCR. *PYK1*, *RPL3*, *YEF3*, *PMA1*, and *ADH1* mRNAs have half-lives within the range of 5 and 50 min [80], which allows relatively accurate measurements without the need for prolonged incubation with thiolutin. HU treatment significantly destabilized all tested mRNAs in WT cells. The effect of HU on mRNA stability in *mec1Δsm11Δ* cells was attenuated for *PYK1* and *RPL3* mRNAs, while the effect on *YEF3*, *PMA1*, and *ADH1* mRNAs did not significantly differ from WT (Fig. 13C). We interpret these results to mean that treatment with HU destabilizes some, perhaps many mRNAs in WT cells, and this destabilizing effect of HU for some mRNAs is attenuated in *mec1Δsm11Δ* cells. Interestingly, HU does not destabilize histone mRNAs, which are produced only during the S phase and are very unstable with have half-lives within 2 and 4 min [81]. Perhaps unstable mRNAs cannot be further destabilized by HU, or destabilization of very short-lived mRNAs cannot be detected by conventional techniques.

The HU-triggered destabilization of mRNAs can be explained by one of the two basic mechanisms. First, HU may activate one or more steps in the mRNA decay pathway, including deadenylation, decapping, and exonucleolytic degradation in 5' to 3' and/or 3' to 5' direction. Second, HU may alter mRNA processing in a way that makes mRNAs more susceptible to degradation. For example, the nascent mRNAs may not contain the normal cap structure (5'-m⁷GpppN) at the 5' end or the poly(A) tail at the 3' end may not be sufficiently long to prevent subsequent exonucleolytic degradation from

the 3' end or decapping and exonucleolytic degradation from the 5' end. To address these possibilities, we determined the HU effect on *YEF3* mRNA stability in *pan2Δ*, *ccr4Δ*, *dcp2Δ*, *xrn1Δ*, and *rat1-1* cells. Pan2p and Ccr4p are subunits of the Pan2p-Pan3p and Ccr4p-Pop2p-Not deadenylases, respectively. Dcp2p is a subunit of Dcp1p-Dcp2p decapping complex and Xrn1p and Rat1p are two major 5' to 3' exonucleases [89]. While HU destabilized *YEF3* mRNA in *pan2Δ* and *ccr4Δ* cells to the same extent as in WT cells, HU did not affect *YEF3* mRNA half-lives in *dcp2Δ* and *xrn1Δ* cells and the effect was significantly attenuated in *rat1-1* cells (Fig. 13D). Since the HU effect on mRNA stability requires the decapping complex Dcp1p-Dcp2p, we conclude that mRNAs produced in the presence of HU contain a normal cap structure at the 5' end that protects them from decay from the 5' end. These results are consistent with a model in which mRNAs produced in the presence of HU contain shorter poly(A) tails that do not require deadenylation for subsequent degradation, or that a decay step subsequent to deadenylation is activated by HU.

Discussion

Perhaps the most surprising and significant finding of this study is that treatment with HU causes accumulation of Rpb1p in the 3' ends of the coding sequences of *PYK1*, *YEF3*, *RPL3*, *ADH1*, and *PMA1* genes, and this phenotype is exacerbated in *mec1Δsml1Δ* cells (Fig. 12A). Even though the increased Rpb1p occupancy in the ends of CDS is a telltale sign of inappropriate transcriptional initiation from within coding regions, we found that except for *YLR454* gene, HU does not cause cryptic transcription in WT cells.

Another possibility that may explain the HU-triggered accumulation of Rpb1p at the 3' ends of CDS and 3'-UTR is a defect in dissociation of RNAPII from chromatin when RNAPII transcribes over the polyadenylation (pA) site, called transcriptional termination. The pA sequence is recognized by the multi-component complexes cleavage and polyadenylation factor (CPF) and cleavage factor (CF), consisting of cleavage factors IA and IB (CFIA and CFIB) [90-92]. The CPF subunit Ysh1p/Brr5p is the endonuclease that cleaves the nascent RNA. The resulting 3' end of the RNA is polyadenylated and the resulting poly(A) tail binds poly(A) -binding proteins, which protect the RNA from exonucleolytic degradation and facilitate nuclear export and translation [93]. The new 5' end of the RNA created by the cleavage of the nascent transcript is not protected by the cap structure and is degraded by Rat1p exonuclease, which catches up with RNAPII and displaces it from chromatin. Strong evidence indicates that this mechanism, referred to as torpedo model, cooperates with the allosteric model. The allosteric model posits that the conformation of RNAPII changes after passage of the pA site, most likely due to recruitment of the CPF and CF, and/or loss of elongation factors [94, 95]. In addition, RNAPII often pauses downstream of the pA site [88, 96]. Interestingly, DDR globally inhibits pre-mRNA 3' end processing in both yeast and human cells [97-99]. In many genes that have multiple pA sites, DDR-mediated inhibition of CPF and CF leads to changes in usage of these alternative pA sites, resulting in preference for longer transcripts [100]. We believe that HU treatment compromises transcriptional termination and enhances RNAPII stalling around the pA site, leading to Rpb1p accumulation at the 3' ends of genes (Fig. 12A). This accumulation is exacerbated in *mec1Δsm11Δ* cells, indicating that Mec1p has a role in transcriptional termination. It would be tempting to

speculate that at least one of the subunits of CPF, CF or Rat1p is regulated by Mec1p phosphorylation. This is an appealing hypothesis, since Mec1p activation during replication stress would at least partly counteract the effect of HU on RNAPII occupancy at the 3' end of genes and would contribute to efficient transcriptional termination, limiting association of RNAPII with chromatin and possible replication-transcription conflicts.

It is also possible that HU-mediated Rpb1p accumulation in the 3' ends of genes is associated with altered pre-mRNA 3' end processing, resulting in mRNAs destabilization. DNA damage response to genotoxic chemicals, including HU, includes degradation of several key subunits of the mRNA 3'-end processing complex, inhibition of mRNA 3'-end cleavage and processing, and altered selection pattern of pA sites, favoring longer transcripts [99, 100]. Since pre-mRNA polyadenylation is dependent on CPF and CF [101-104], it is possible that HU treatment affects not only pA site selection, but also shortens the length of the poly(A) tail, resulting in less stable mRNAs. This notion is consistent with our observation that deadenylation of mRNAs by Pan2p-Pan3p and Ccr4p-Pop2p-Not deadenylases is not required for destabilizing effect of HU (Fig. 13D).

Overall, our data show that HU globally inhibits RNA synthesis by RNAPI, RNAPII, and RNAPIII. HU triggers RNAPII accumulation in the 3' ends of CDS and 3'-UTR, probably due to inhibition of mRNA 3'-end cleavage and processing under genotoxic conditions [99]. This mechanism may also be responsible for HU-mediated destabilization of mRNAs. The RNAPII accumulation in the 3' ends of genes is opposed by Mec1p, suggesting that Mec1p affects transcriptional termination.

Materials and Methods

Yeast Strains and Media

All yeast strains are listed in Table 1. Standard genetic techniques were used to manipulate yeast strains and to introduce mutations from non-W303 strains into the W303 background [112]. Cells were grown in YPD medium (1% yeast extract, 2% Bacto peptone, 2% glucose) or YPR medium (1% yeast extract, 2% Bacto peptone, 2% raffinose). Expression of *GALI-YLR454* construct was induced by adding 2% galactose for 2 h to cells grown in YPR medium.

4tU labeling and purification of nascent RNA

S. cerevisiae and *S. pombe* nascent RNA was labeled with 4-thiouracil (4tU) as previously described [113, 114]. Briefly, *S. cerevisiae* cultures were grown in 30 ml of YPD medium at 30°C to log phase ($A_{600\text{nm}} \sim 0.8$). In parallel, wild type *S. pombe* cells were grown in 30 ml of YES medium at 32°C, also to log phase ($A_{600\text{nm}} \sim 0.8$). Newly synthesized RNA in both *S. cerevisiae* and *S. pombe* was labeled for 6 min with 5 mM 4tU. For treated samples, 200 mM HU was added to *S. cerevisiae* 30 min before labeling. After labeling, cells were pelleted and stored at -70°C. *S. cerevisiae* and *S. pombe* cells were mixed in 3:1 ratio and RNA was extracted and purified using RNeasy kit (74106, Qiagen). None of the solutions used for extraction and purification of RNA contained dithiothreitol or 2-mercaptoethanol. After isolation, 200 µg of the 4tU-labeled RNA dissolved in 100 µl of DEPC-treated RNase free water were incubated at 60°C for 10 min and cooled down on ice for 2 min. Subsequently, 600 µl of DEPC-treated RNase free water were added, followed by 100 µL of biotinylation buffer (100 mM Tris- HCl pH

7.5, 10 mM EDTA) and 200 μ L of 1 mg/mL EZ-link HPDP Biotin (A35390, ThermoFisher). The mixture was incubated for 20 min at 65°C at 300 rpm protected from light in Eppendorf Thermomixer C. The RNA was phenol-chloroform extracted to remove unincorporated biotin and isopropanol precipitated. The RNA was re-suspended in 100 μ L DEPC-treated RNase-free water. Meanwhile, 50 μ l of μ MACS streptavidin microbeads (130-074-101, Miltenyi Biotec) were equilibrated with 500 μ l washing buffer (100 mM Tris-HCl at pH 7.5, 10 mM EDTA, 1M NaCl, 0.1% Tween20) containing 20 μ g of glycogen for 30 min with gentle shaking. Beads were applied to μ column placed in a magnetic stand. After the liquid has drained from the column, the column was removed from the stand and the beads were eluted with 100 μ l of the washing buffer. Biotinylated RNA was denatured at 65°C for 10 min, cooled down for 5 min on ice and incubated with 100 μ L of the equilibrated μ MACS streptavidin microbeads for 90 min at room temperature with gentle shaking. The microbeads were pipetted to the columns in the magnetic stand, the flow through was reapplied, and the microbeads were washed five times with increasing volumes of washing buffer (600, 700, 800, 900, and 1000 μ L). Ultimately, labeled RNA was eluted twice with 200 μ L of 0.1 M dithiothreitol and precipitated overnight in 1/10 volume of 3 M NaOAc, 3 volumes of 100% ice cold ethanol and 20 μ g of glycogen. The nascent RNA was recovered by centrifugation and resuspended in 60 μ L of DEPC-treated RNase-free water.

Slot blot analysis of biotinylated RNA

S. cerevisiae cells were grown, labeled with 4tU, and the RNA isolated and purified as described above. For treated samples, 200 mM HU was added to the

cultures 30 min before labeling. RNA was biotinylated using iodoacetyl-biotin (21333, ThermoFisher Scientific), phenol-chloroform extracted, and purified with RNeasy kit (74106, Qiagen). Slot blot assay was performed as described [115]. Zeta membrane (162-0153, BioRad) was incubated in nuclease-free water for 10 min and assembled in Bio-Dot SF apparatus (162-0161, BioRad). RNA samples were prepared using ice-cold binding buffer (10 mM NaOH, 1 mM EDTA) and applied to the membrane. Wells were rinsed with cold binding buffer and excess buffer was removed by vacuum. RNA was crosslinked to the membrane with UV light at 120 mJoule/cm² for 45 s. Membrane was washed in blocking buffer (0.5 X PBS, 10 % SDS, 1 mM EDTA) for 30 min, incubated with 1:1000 streptavidin-horseradish peroxidase (HRP; SA-5004-1; Vector Laboratories) for 15 min and washed six times with PBS containing decreasing concentrations of SDS (10%, 1% and 0.1%, twice each). Membrane-bound HRP was visualized using enhanced chemiluminescence.

Real-time RT-qPCR

The procedures to extract total RNA from yeast cells and perform RT-qPCR were as previously described [105, 116]. The primers used for RT-qPCR are listed in Table 2.

mRNA decay rates

The half-lives ($t_{1/2}$) of mRNAs were determined using transcriptional shut off with thiolutin as described [81, 117, 118]. Yeast cells were inoculated to an $A_{600} = 0.1$ and grown in YPD medium to an $A_{600} = 0.8$. Thiolutin was added to 8 $\mu\text{g/ml}$ and culture samples were removed during 0 – 120 min incubation. Total RNA was isolated as

described above and mRNA levels were determined by RT-qPCR using *RDN25* RNA for normalization. The half-lives of individual mRNAs were determined in Microsoft Excel from logarithmic plots of each remaining mRNA at different times after the transcriptional shutoff.

ChIP assays

In vivo chromatin crosslinking and immunoprecipitation were performed essentially as described [116]. Immunoprecipitation was performed with the following antibodies: anti-RNAPII Rpb1p monoclonal antibody (8WG16; 664912, BioLegend), anti-myc monoclonal antibody (9B11; 2276S; Cell Signaling), and anti-HA monoclonal antibody (F-7; sc-7392; Santa Cruz Biotechnology). The primers used for qPCR are listed in Table 3.

Statistical analysis

The results represent at least three independent experiments. Numerical results are presented as means \pm standard deviations (SD). Data were analyzed by using an InStat software package (GraphPAD, San Diego, CA, USA). Statistical significance was evaluated by one-way analysis of variance, and $p < 0.05$ was considered significant.

Table 1 Yeast strains used in this study

Strain	Genotype	Source/Ref.
W303-1a	<i>MATa ade2-1 his3-11,15 leu2-3,112 trp1-1 ura3-1 ssd1-d2 can1-100</i>	R. Rothstein
W303-1α	<i>MATα ade2-1 his3-11,15 leu2-3,112 trp1-1 ura3-1 ssd1-d2 can1-100</i>	R. Rothstein
W303	<i>MATa/MATα ade2-1/ade2-1 his3-11,15/his3-11,15 leu2-3,112/leu2-3,112 trp1-1/trp1-1 ura3-1/ura3-1 can1-100/can1-100</i>	R. Rothstein
SN141	<i>MATa ade2-1 his3-11,15 leu2-3,112 trp1-1 ura3-1 ssd1-d2 can1-100 dun1::HIS3</i>	This study
SN159	<i>MATa ade2-1 his3-11,15 leu2-3,112 trp1-1 ura3-1 ssd1-d2 can1-100 tell::HIS3</i>	105
SN136	<i>MATα ade2-1 his3-11,15 leu2-3,112 trp1-1 ura3-1 ssd1-d2 can1-100 chk1::HIS3</i>	105
SN117	<i>MATa ade2-1 his3-11,15 leu2-3,112 trp1-1 ura3-1 ssd1-d2 can1-100 mecl::HIS3 sml1::KAN</i>	105
LG606	<i>MATa ade2-1 his3-11,15 leu2-3,112 trp1-1 ura3-1 ssd1-d2 can1-100 rad53::KAN sml1::HYG</i>	105
AD066	<i>MATα ade2-1 his3-11,15 leu2-3,112 trp1-1 ura3-1 ssd1-d2 can1-100 SPT15-3HA::URA3</i>	106
MB163	<i>MATa ade2-1 his3-11,15 leu2-3,112 trp1-1 ura3-1 ssd1-d2 can1-100 mecl::HIS3 sml1::KAN SPT15-3HA::URA3</i>	81
MB123	<i>MATa ade2-1 his3-11,15 leu2-3,112 trp1-1 ura3-1 ssd1-d2 can1-100 pan2::URA3</i>	81
SM096	<i>MATa ade2-1 his3-11,15 leu2-3,112 trp1-1 ura3-1 ssd1-d2 can1-100 ccr4::URA3</i>	81
MB129	<i>MATa ade2-1 his3-11,15 leu2-3,112 trp1-1 ura3-1 ssd1-d2 can1-100 dcp2::HIS3</i>	This study
MB115	<i>MATa ade2-1 his3-11,15 leu2-3,112 trp1-1 ura3-1 ssd1-d2 can1-100 xrn1::URA3</i>	81
MB153	<i>MATa ade2-1 his3-11,15 leu2-3,112 trp1-1 ura3-1 ssd1-d2 can1-100 spt21::HIS3</i>	This study
MZ672	<i>MATa ade2-1 his3-11,15 leu2-3,112 trp1-1 ura3-1 ssd1-d2 can1-100 spt10::KAN</i>	107
SJ027	<i>MATa ade2-1 his3-11,15 leu2-3,112 trp1-1 ura3-1 ssd1-d2 can1-100 rad9::KAN</i>	This study
SJ015	<i>MATa ade2-1 his3-11,15 leu2-3,112 trp1-1 ura3-1 ssd1-d2 can1-100 mrcl::KAN</i>	This study
MZ576	<i>MATa ade2-1 his3-11,15 leu2-3,112 trp1-1 ura3-1 ssd1-d2 can1-100 asf1::HIS3</i>	108
MZ642	<i>MATa ade2-1 his3-11,15 leu2-3,112 trp1-1 ura3-1</i>	108

MZ533	<i>ssd1-d2 can1-100 rtt106::KAN MATa ade2-1 his3-11,15 leu2-3,112 trp1-1 ura3-1 ssd1-d2 can1-100 cac1::LEU2</i>	108
MZ700	<i>MATa ade2-1 his3-11,15 leu2-3,112 trp1-1 ura3-1 ssd1-d2 can1-100 hir1::HIS3</i>	108
CMY125	<i>MATa his3-Δ1 leu2-Δ0 met15-Δ0 ura3-Δ0 P_{GALI}- YLR454_w</i>	109
SN691	<i>MATa ade2-1 his3-11,15 leu2-3,112 trp1-1 ura3-1 ssd1-d2 can1-100 P_{GALI}-YLR454_w</i>	This study
SN684	<i>MATa ade2-1 his3-11,15 leu2-3,112 trp1-1 ura3-1 ssd1-d2 can1-100 mec1::HIS3 sml1::KAN P_{GALI}- YLR454_w</i>	This study
YSB1796	<i>MATa ura3-52,leu2Δ1, trp1Δ63,his3ΔLEU2/KanR, rat1-1-TAP::HIS3</i>	110
JS311- A190MN	<i>MATa his3Δ200,leu2Δ1,met15Δ0, trp1Δ63,ura3-167, RDNI::Ty1-MET15,mURA3/HIS3; RPA190-MNase-3X-HA::KanMX6</i>	59
RET1- 13MYC	<i>MATa his3Δ1 leu2Δ0 lys2Δ0 ura3Δ0 RET1-13MYC-KanMX</i>	111

Table 2 Mammalian Primer sequences for RT-qPCR

Primer Name	Forward (5'→3')	Reverse (5'→3')
18S	CGGCTACCACATCCAAGGAA	GCTGGAATTACCGCGGCT
Bach1	TGCGATGTCACCATCTTTGT	CCTGGCCTACGATTCTTGAG
HO-1	AAGACTGCGTTCCTGCTCAAC	AAGCCCTACAGCAACTGTCTG
HK2	GAGCCACCACTCACCTACT	CCAGGCATTCGGCAATGTG
GAPDH	GGAGCGAGATCCCTCCAAAAT	GGCTGTTGTCATACTTCTCATGG
NDUFB5	AGCTGGAAGTGCGAAAATTGA	ATACCAGGGTCCATCTCCTCT
COX15	CAGCGCCTAGAGCACAGTG	GCCAGACTCTGTCAACCTAGT
COX17	TGCGTGTATCATCGAGAAAGGA	GCCTCAATTAGATGTCCACAGTG
ATP5D	CCCTCCTTGGTCAAGAGCAC	GTATCTCCGGTCGTTTCAGCA
SLC25A15	CCTGAAGACTTACTCCCAGGT	GCGATGTTGGCGATTAGTGC
Catalase	TGGAGCTGGTAACCCAGTAGG	CCTTTGCCTTGGAGTATTTGGTA
MMP1	GCGCACAAATCCCTTCTACC	ATCCGTGTAGCACATTCTGTCC
MMP9	ATTTCTGCCAGGACCGCTTCTAC	ATCCGGCAAACCTGGCTCCTTC
MMP13	TGCAGAGCGCTACCTGAGATCATA	GGAGCTTGCTGCATTCTCCTTCA
CXCR4	TCTTCCTGCCACCATCTACTC	TGCAGCCTGTACTTGTCCGTC
Vimentin	CAGGCAAAGCAGGAGTCCA	AAGTTCTCTTCCATTCACGCA

Table 3 Yeast Primer sequences for RT-qPCR

Primer Name	Forward (5'→3')	Reverse (5'→3')
SNR52	TGATGAATGACATTAGCGTGAACA	GAAGGAAGGCAACATAAGTTTTTCT
RPR1	CCACCTATGGGCGGGTTATC	AGGCCGAACTCCGTGAATTT
SUP4	TCGGTAGCCAAGTTGGTTTAAGG	TCTCCCGGGGGCGAGTC
SPTUB	CCGCTGGTGAAAGTATGTT	GCCAATTCAGCACCTTCAGT
SCR1	CCTTTGGGCAAGGGATAGTT	TTACGACGGAGGAAAGACG
SNR6	CGAAGTAACCCTTCGTGGAC	TCATCCTTATGCAGGGGAAC
YEF3	ATCTGTTGCCACTGCTGACA	TAGCAGCGGTCTTCTTGTC
RPL3	AGAGAGCTGCCTCCATCAGA	CAGCTTCGACAACTTCACGC
PYK1	TTGTTGCTGGTTCTGACTTGAG	CAATGTTCAAACCAGCCTTTCTC
25S	GGAATGTAGCTTGCCTCGGT	TTACGTTCGAGTCCTCAGTC
5S	ACCAGAAAGCACCGTTTCCC	GCACCTGAGTTTCGCGTATG
FLO8-5' region	CCCACGGAACAACCGTACAT	TCCGAATTTTCCGCCGTAGG
FLO8-3' region	TGTGGGTACAACCTTTGGGTCC	ATCCGGTCCTTGGTCTTCAA
VPS72-5' region	TCTAGGAGGTCTAATGCCGGT	TCTTCCTGAAACAACAGCCCT
VPS72-3' region	CCAAGGACTGGTGTGCCTTA	TACCGCCGTTTTTGAACCCA
PMA1-2	GTGTCGACGACGAAGACAGT	ACCGTAAGATGGGTCAGTTTGT
PMA1-6	AAGTGTGGAAGACTTCATGGCT	AATGCTACTTCAACAGGATTAGGT
ADH1-2	ACGAATCCCACGGTAAGTTGG	CAGTGTGACAGACACCAGAGT
ADH1-4	CGTCGGTAACAGAGCTGACA	GCAAGGTAGACAAGCCGACA
PYK1-2	ACGTTGTTGCTGGTTCTGAC	CCAGCCTTTCTCAAAGCAACC
PYK1-4	AGCCCGTATCAACTTCGGTA	TGTTGGAGTGACCAGCACC
RPL3-2	AGTACGAAGCACCACGTCAC	AGCAACTGGCTTGGATCTGT
RPL3-5	TGGTTTCGTCCACTACGGTG	AGCTGACTTCTTCAAAGCCT
YEF3-2	ATCTGTTGCCACTGCTGACA	TAGCAGCGGTCTTCTTGTC
YEF3-7	CCGGTACATGGCAAAGACCT	TTGACGGCCCAGACTTCTC
YLR454w-1	ACCGTCAGGCTAAAATCCGT	AGCCCCACCATTATCTTCG
YLR454w-5	TCCAACCAAACCTTGAGGGTCA	TGGTGAAGTGTCGTCAGCAA

Table 4 Primer sequences for ChIP assays

Primer name	Forward (5'→3')	Reverse (5'→3')
PMA1-1	CCAATTATGACCGGTGACGAAA	ATCGAAACTAATGGAGGGGAGC
PMA1-2	GTGTGACGACGAAGACAGT	ACCGTAAGATGGGTGAGTTTGT
PMA1-3	ACGAAGTCGTCCAGGTGA	TGGTCACCGTAATGTTTGTGCG
PMA1-4	CCAGCTGTCGTTACCACCAC	GATTTGACACCAGCCAAGG
PMA1-5	ATGCTTTGAAGACCTCCAGAC	AGCAATCCATAGACCCAAGAAGA
PMA1-6	AAGTGTGGAAGACTTCATGGCT	AATGCTACTTCAACAGGATTAGGT
PMA1-7	AGCCAACAAGAATAAGCCGC	AAATTTTAAGGTGTGTGTGTGGA
PMA1-8	TGCAAGATGTTTGTATAGAGGGAC A	AGAAGAGCTGGGCAGGAACT
PMA1-9	CTCGCTTACGTTTATGCGCC	GGAGGCGGCCTTCAATCAT
ADH1-1	ACAGCACCAACAGATGTCGT	AAGGCCGTATACCGTTGCTC
ADH1-2	ACGAATCCCACGGTAAGTTGG	CAGTGTGACAGACACCAGAGT
ADH1-3	GTCTGCTAACTTGATGGCCG	TCACCACCGTCAATACCCAA
ADH1-4	CGTCGGTAACAGAGCTGACA	GCAAGGTAGACAAGCCGACA
ADH1-5	GGTCAGGTTGCTTTCTCAGG	GGGTGAAATGGGGAGCGATT
PYK1-1	TCCTTTCCTTCCCATATGATGCT	GGTTCTTGAAATGAAAAGTTACC A
PYK1-2	ACGTTGTTGCTGGTTCTGAC	CCAGCCTTCTCAAAGCAACC
PYK1-3	TTCATCAGAACCGCCAACGA	TGGCAACCATAACACCGTCA
PYK1-4	AGCCCGTATCAACTTCGGTA	TGTTGGAGTGACCAGCACC
PYK1-5	AGACATGGTTTTTCTTTTCAACTCA	CCAAAAATGCAACACCTCATCG
PYK1-6	GGATGGCGAAAGGATACGCT	AACGAAGGCCAGAAGCTGAA
YEF3-1	CCCACCCATGCATAACCCTA	AGATAATTATACTCGAGGAAGCGA A
YEF3-2	ATCTGTTGCCACTGCTGACA	TAGCAGCGGTCTTCTTGTC
YEF3-3	GGAAGTCAAGGCTGCTGCTA	GGAACTTCAGTTGGGTGAGC
YEF3-4	ATTGCTGACCCAGAAGCCAG	AGCAACGGTTTCGTCCTCA
YEF3-5	TGCTTTGTCTGGTGGTTGGA	ACCAAGCAACGTTGACGGTA
YEF3-6	GCCGGTATCCACTCCAGAAG	ACGGACATCATTGGAACCCA
YEF3-7	CCGGTACATGGCAAAGACCT	TTGACGGCCAGACTTCTTC
YEF3-8	AAAGCGTTCATTAGTCAGACA	ACCGAAAAGGGTATGAGGCA
RPL3-1	ACTCACGCACACTGGAATGA	GAAAAACAGTTGTGCGTCGCT
RPL3-2	AGTACGAAGCACCACGTCAC	AGCAACTGGCTTGGATCTGT
RPL3-3	AAGTACGCTTCCGTCGTCAG	TCGAAATGTTACGAGCCCA

RPL3-4	AAGGGTCACGGTTTCGAAGG	CCACATAACGTGGGCTGGAT
RPL3-5	TGGTTTCGTCCACTACGGTG	AGCTGACTTCTTCCAAAGCCT
RPL3-6	GACCCGCATGCGATTATGTT	GAGGTCCAAGTCAAACGGC
YLR454w-1	ACCGTCAGGCTAAAATCCGT	AGCCCCACCATTATCTTCG
YLR454w-2	GGCCGTCTCAGGAATACACA	ACTCCTTTAGTTGGCCCCAT
YLR454w-3	TTACTCGTTGTTCGTGCCCA	GAACCACCCCAAGTTACTCGT
YLR454w-4	CTTTAGCAAGTGGAAGGGC	TGCTTTGTCTGTTCTTCTGGT
YLR454w-5	TCCAACCAAACCTTTGAGGGTCA	TGGTGAAGTGTCTGTCAGCAA
YLR454W-6	AAACAAGGTCACACGAAAACCA	TGCCTTAGTTATCGTTCAAATGC
POL1N	TGGTAGGCTGATATGTGATATCGC	AACGGCTTATGCTCCTTTTCAC
RDN37-1	CGGGGCACCTGTCACTTT	TCTTTTGCCTCTCTGTCTGC
RDN37-2	GCAGAGAGACCTGAAAAAGCA	CTACTGGCAGGATCAACCAGA
RDN37-3	AACCTTGAGTCCTTGTGGCT	ACCAACAAAATAGAACCAAACGT
RDN37-4	GGTTTCAAGCCGATGGAAGT	CCAAGGTTAGACTCGCTGGC
RDN37-5	TTAAGTGCGCGGTCTTGCTA	CGATTGCTCGAATGCCAAA
RDN37-6	AACGGATCTCTTGGTTCTCG	GTGCGTTCAAAGATTCGATG
RDN37-7	GGTTTCTCTGCGTGCTTGAG	ATTGTTGCGCTAGACGCTCTC
RDN37-8	GGGCATTGATCAGACATGGT	GGCAGTATTCCCACAGGCTA
RDN37-9	AACAGCTTATCACCCCGGAA	TGCGGTTATCAGTACGACCT
RDN37-10	TCTGCTGAGATTAAGCCTTTGT	TTCTCTCTAAACTAGGCCCCG
RDN37-11	AAGATGGGTTGAAAGAGAAGGG	TCATATCAAAGGCATGTCCTGT
SNR52	TGATGAATGACATTAGCGTGAACA	GAAGGAAGGCAACATAAGTTTTTC T
RPR1	CCACCTATGGGCGGGTTATC	AGGCCGAACTCCGTGAATTT
SUP4	TCGGTAGCCAAGTTGGTTTAAAGG	TCTCCCGGGGGCGAGTC
SCR1	CCTTTGGGCAAGGGATAGTT	TTACGACGGAGGAAAGACG
SNR6	CGAAGTAACCCTTCGTGGAC	TCATCCTTATGCAGGGGAAC
HYP2	TGAAACTGCTGACGCTGGTT	ACTTTAGCGTGACCGTGCTT
PGK1	TGGACTTGAAGGACAAGCGT	GATGGTTGGCAAAGCAGCAA
ACT1	TATGTGTAAAGCCGGTTTTGC	GACAATACCGTGTTCAATTGGG
5S	ACCAGAAAGCACCGTTTCCC	GCACCTGAGTTTCGCGTATG
MUP1	CAACGGTGCCTCCGATTTTG	GAGGAAACGGCGAAAACACC
PDC1	ATTGCCGGTTCTTACGCTGA	TCACCGTTACCCAAGGTGTG
EDC1	GCGAGGGGAAATGCTGCTAA	GGGAAGAAGGTGGAGAGTGC

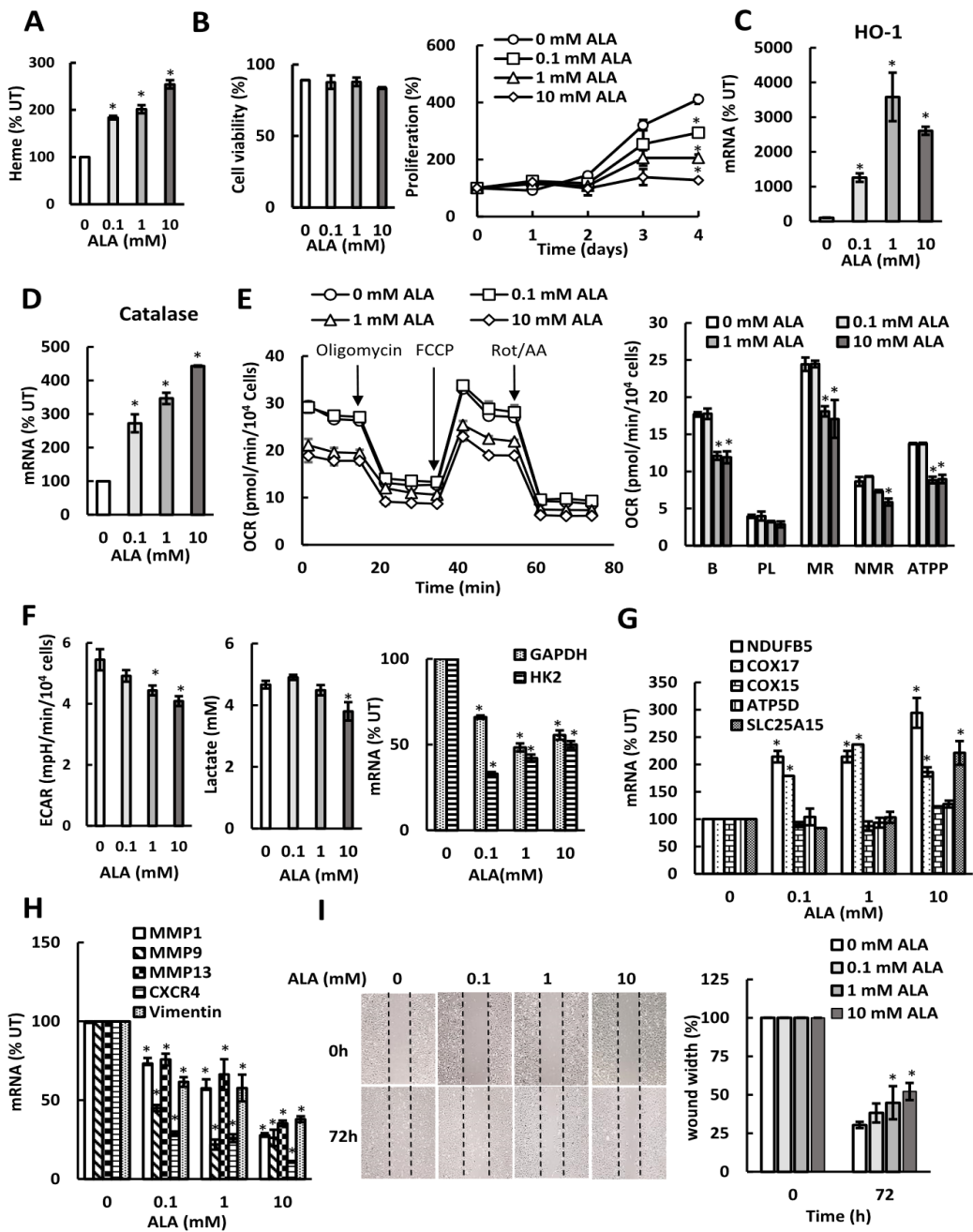


Figure 1. ALA inhibits mitochondrial respiration and aerobic glycolysis in SKOV3 cells.

(A) Cellular heme levels in SKOV3 cells treated with ALA. Results are shown in comparison with untreated cells (%UT; 0 mM ALA). (B) Cell viability and proliferation. (C) HO-1 and (D) catalase mRNA analyzed by qRT-PCR in SKOV3 cells treated with ALA for 24 h. (E) Oxygen consumption rate (OCR) was measured in SKOV3 cells treated with ALA for 24 h. OCR was measured under basal conditions followed by the sequential addition of oligomycin (1.5 μ M), FCCP (0.5 μ M), and rotenone & antimycin A (Rot/AA; 0.5 μ M) as indicated. Each data point represents an OCR measurement. Derived respiratory parameters are basal respiration (B), proton leak (PL), maximal respiration (MR), non-mitochondrial respiration (NMR), and ATP production (ATPP). (F) Extracellular acidification rate (ECAR), lactate accumulation in the medium, and GAPDH and HK2 mRNA levels in SKOV3 cells treated with ALA for 24 h. (I) Expression of metastatic genes in SKOV3 cells treated with ALA for 24 h. (G) Expression of ETC and OXPHOS genes measured by RT-PCR in SKOV3 cells treated with ALA for 24 h. (H) Expression of metastatic genes in SKOV3 cells treated with ALA for 24 h. (I) Migration of SKOV3 cells treated with ALA for 72 h analyzed by wound healing assay (n = 3, magnification: \times 10). (A-I) The experiments were repeated three times, and the numerical results are shown as means \pm S.D. Values that are statistically different ($p < 0.05$) from the control (untreated cells) are indicated by an asterisk.

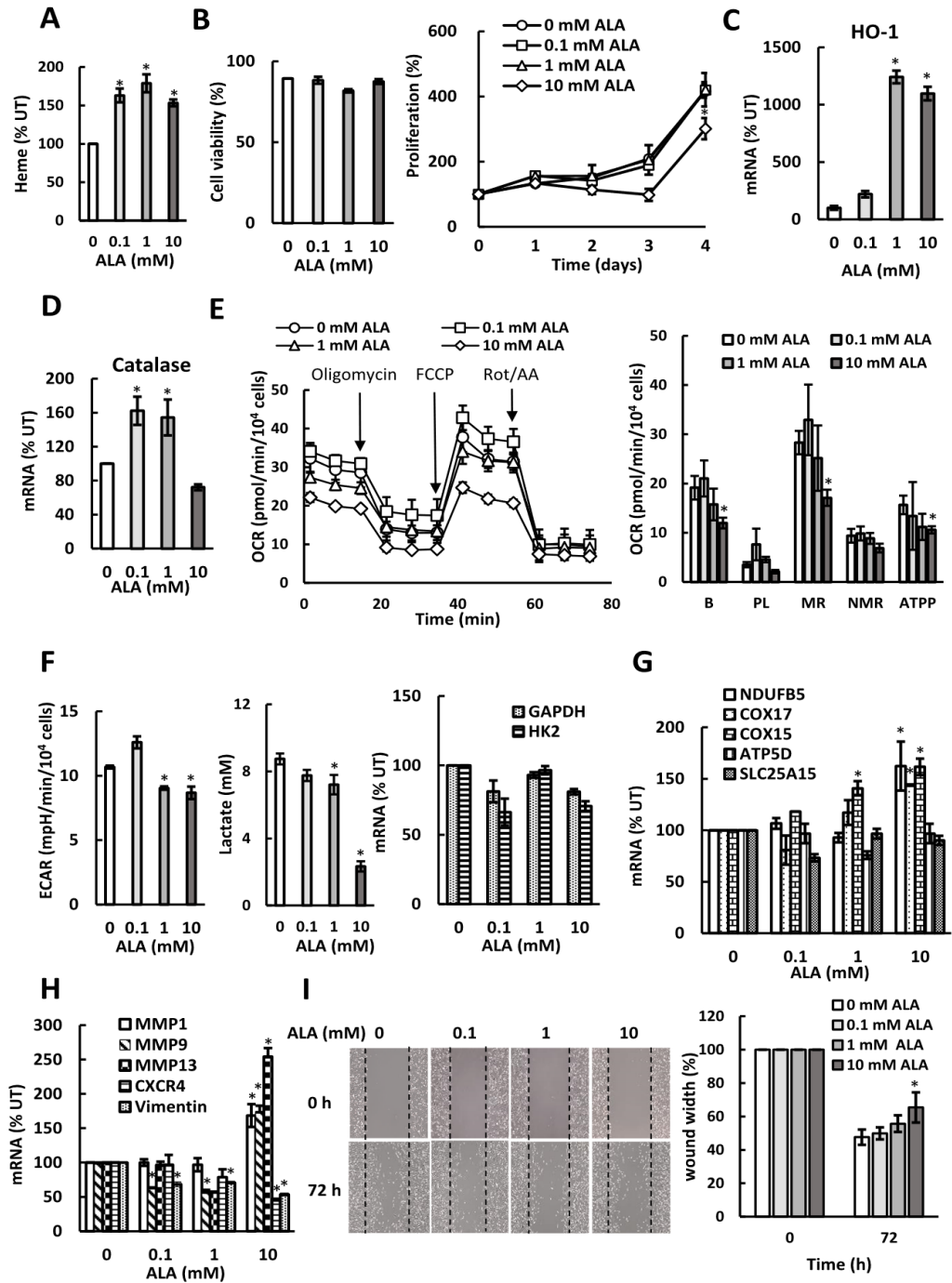


Figure 2. ALA inhibits mitochondrial respiration and aerobic glycolysis in MDA MB 231 cells.

(A) Cellular heme levels and (B) cell viability and proliferation in MDA MB 231 cells treated with ALA. (C) HO-1 and (D) catalase mRNA analyzed by qRT-PCR in MDA MB 231 cells treated with ALA for 24 h. (E) OCR was measured in MDA MB 231 cells treated with ALA for 24 h. (F) ECAR, lactate accumulation in the medium, and GAPDH and HK2 mRNA levels in MDA MB 231 cells treated with ALA for 24 h. (G) Expression of ETC and OXPHOS genes in MDA MB 231 cells treated with ALA for 24 h. (H) Expression of metastatic genes in MDA MB 231 cells treated with ALA for 24 h. (I) Migration of MDA MB 231 cells treated with ALA for 72 h analyzed by wound healing assay (n = 3). (A-I) The experiments were repeated three times, and the numerical results are shown as means \pm S.D. Values that are statistically different ($p < 0.05$) from the control (untreated cells) are indicated by an asterisk.

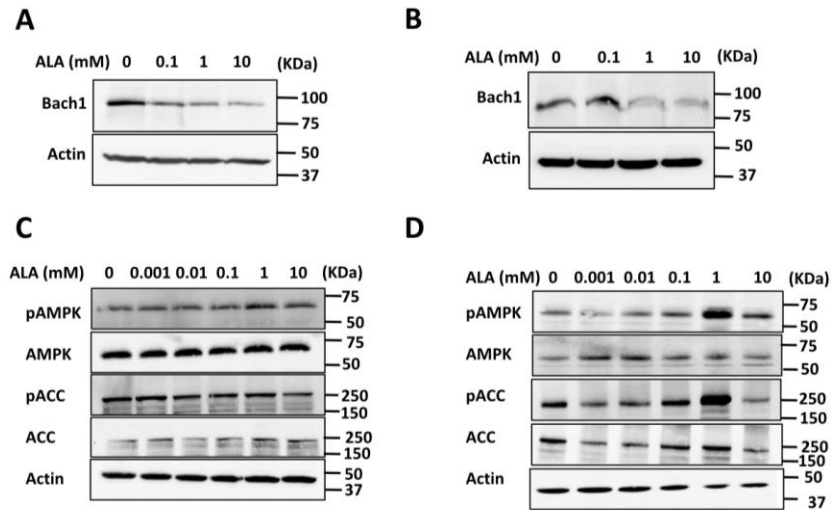


Figure 3. ALA destabilizes Bach1 in SKOV3 and MDA MB 231 cells and activates AMPK in MDA MB 231 cells

(A) SKOV3 and (B) MDA MB 231 cells were treated with 0, 0.1, 1, and 10 mM ALA for 24 h. Whole cell extracts were analyzed by Western blotting using antibodies against Bach1 and actin. (C) SKOV3 and (D) MDA MB 231 cells were treated with 0, 0.001, 0.01, 0.1, 1, and 10 mM ALA for 24 h and whole cell extracts were analyzed by Western blotting using antibodies against pAMPK, AMPK, pACC, ACC, and actin. The figures represent typical results from three independent experiments.

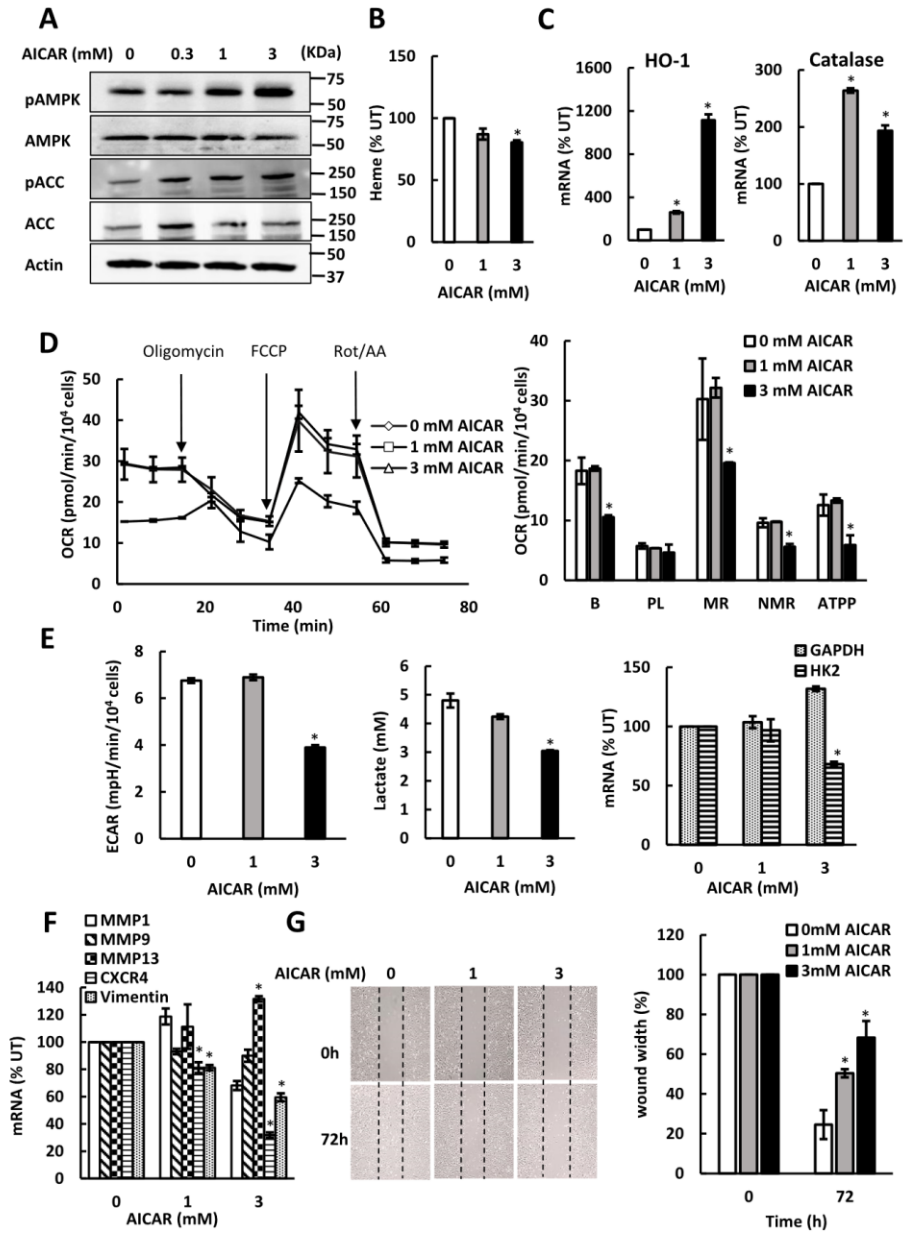


Figure 4. AMPK inhibits mitochondrial respiration and aerobic glycolysis in SKOV3 cells.

(A) SKOV3 cells were treated with 0, 0.3, 1, and 3 mM AICAR for 24 h and whole cell extracts were analyzed by Western blotting using antibodies against pAMPK, AMPK, pACC, ACC, and actin. The figure represents typical results from three independent experiments. (B) Cellular heme levels in SKOV3 cells treated with AICAR. (C) HO-1 and catalase mRNAs were analyzed by qRT-PCR in SKOV3 cells treated with AICAR for 24 h. (D) OCR was measured in SKOV3 cells treated with AICAR for 24 h. (E) ECAR, lactate accumulation in the medium, and GAPDH and HK2 mRNA levels in SKOV3 cells treated with AICAR for 24 h. (F) Expression of metastatic genes in SKOV3 cells treated with AICAR for 24 h. (G) Migration of SKOV3 cells treated with AICAR for 72 h analyzed by wound healing assay ($n = 3$). (A-G) The experiments were repeated three times, and the numerical results are shown as means \pm S.D. Values that are statistically different ($p < 0.05$) from the control (untreated cells) are indicated by an asterisk.

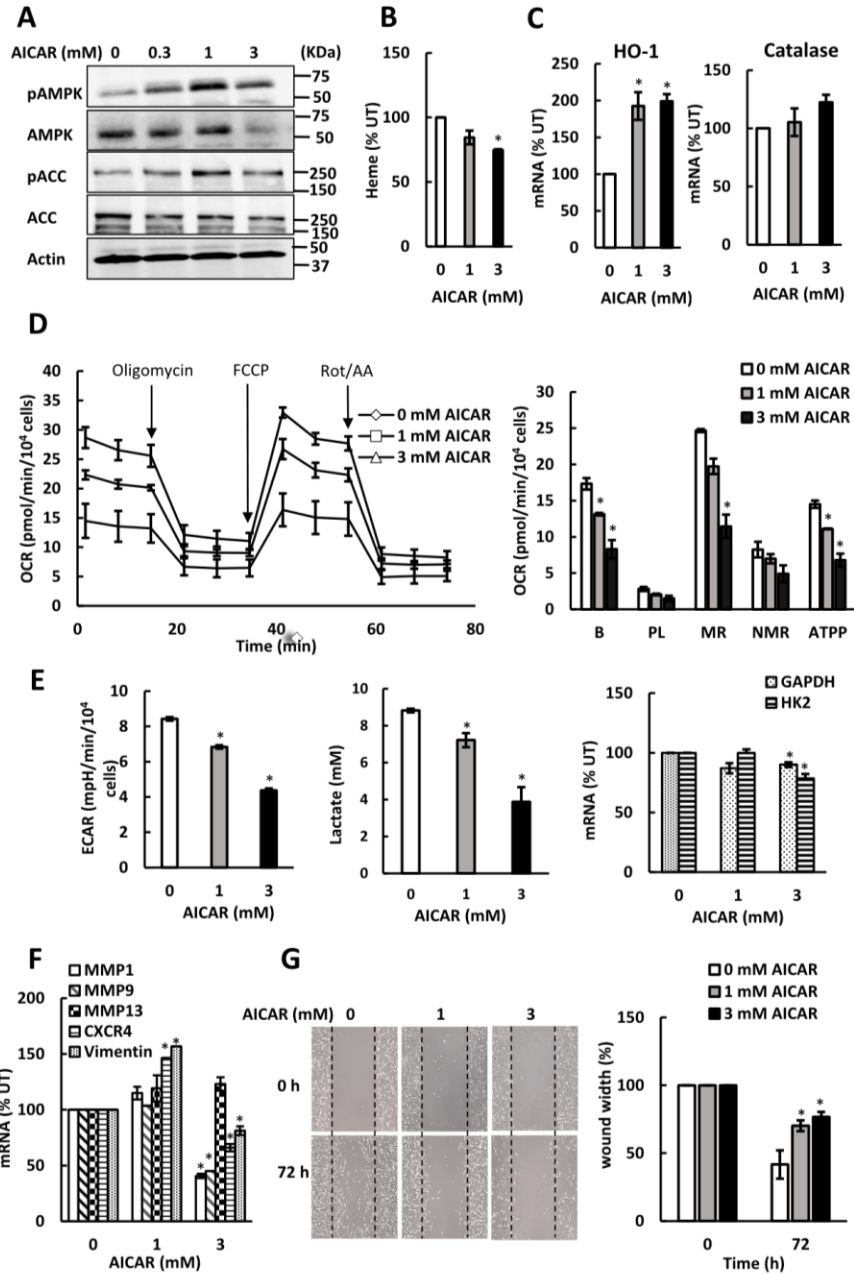


Figure 5. AMPK inhibits mitochondrial respiration and aerobic glycolysis in MDA MB 231 cells.

(A) MDA MB 231 cells were treated with 0, 0.3, 1, and 3 mM AICAR for 24 h and whole cell extracts were analyzed by Western blotting using antibodies against pAMPK, AMPK, pACC, ACC, and actin. The figure represents typical results from three independent experiments. (B) Cellular heme levels in MDA MB 231 cells treated with AICAR for 24 h. (C) HO-1 and catalase mRNAs were analyzed by qRT-PCR in MDA MB 231 cells treated with AICAR for 24 h. (D) OCR was measured in MDA MB 231 cells treated with AICAR for 24 h. The experiment was performed as described in Fig. 1E. (E) ECAR, lactate accumulation in the medium, and GAPDH and HK2 mRNA levels in MDA MB 231 cells treated with AICAR for 24 h. (F) Expression of metastatic genes in MDA MB 231 cells treated with AICAR for 24 h. (G) Migration of MDA MB 231 cells treated with AICAR for 72 h analyzed by wound healing assay (n = 3). (A-G) The experiments were repeated three times, and the numerical results are shown as means \pm S.D. Values that are statistically different ($p < 0.05$) from the control (untreated cells) are indicated by an asterisk.

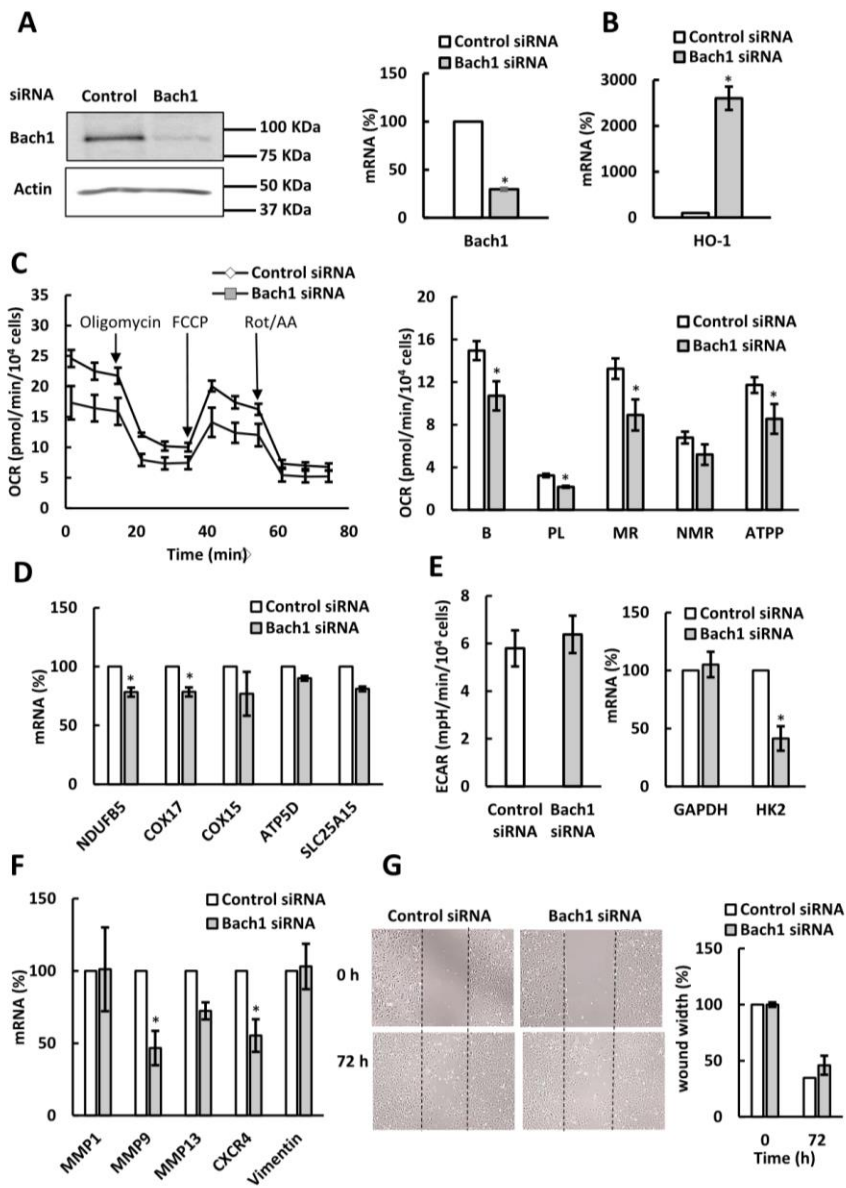


Figure 6. Bach1 regulates mitochondrial respiration in SKOV3 cells.

SKOV3 cells were transfected with Bach1 or control siRNA and analyzed by (A) western blotting using Bach1 and actin antibodies and qRT-PCR. (B) HO-1 mRNA levels, (C) OCR, (D) expression of ETC and OXPHOS genes, (E) ECAR and GAPDH and HK2 mRNA levels, (F) expression of metastatic genes, and (G) migration of SKOV3 cells analyzed by wound healing assay (n = 3). (A-G) The experiments were repeated three times, and the numerical results are shown as means \pm S.D. Values that are statistically different ($p < 0.05$) from the control (SKOV3 cells transfected with control siRNA) are indicated by an asterisk.

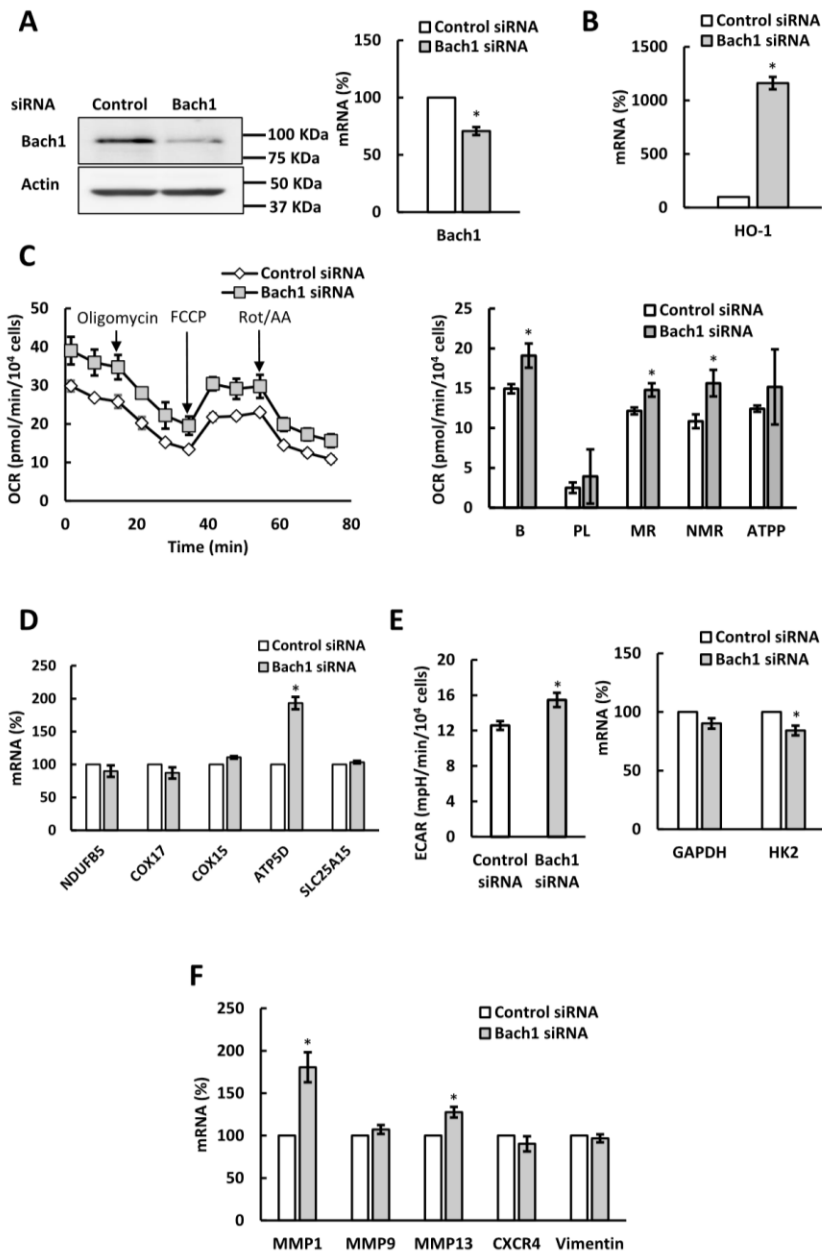


Figure 7. Bach1 regulates mitochondrial respiration in MDA MB 231 cells.

MDA MB 231 cells were transfected with Bach1 or control siRNA and analyzed by (A) western blotting using Bach1 and actin antibodies and qRT-PCR. (B) HO-1 mRNA levels, (C) OCR, (D) expression of ETC and OXPHOS genes, (E) ECAR and GAPDH and HK2 mRNA levels, and (F) expression of metastatic genes. (A-F) The experiments were repeated three times, and the numerical results are shown as means \pm S.D. Values that are statistically different ($p < 0.05$) from the control (MDA MB 231 cells transfected with control siRNA) are indicated by an asterisk.

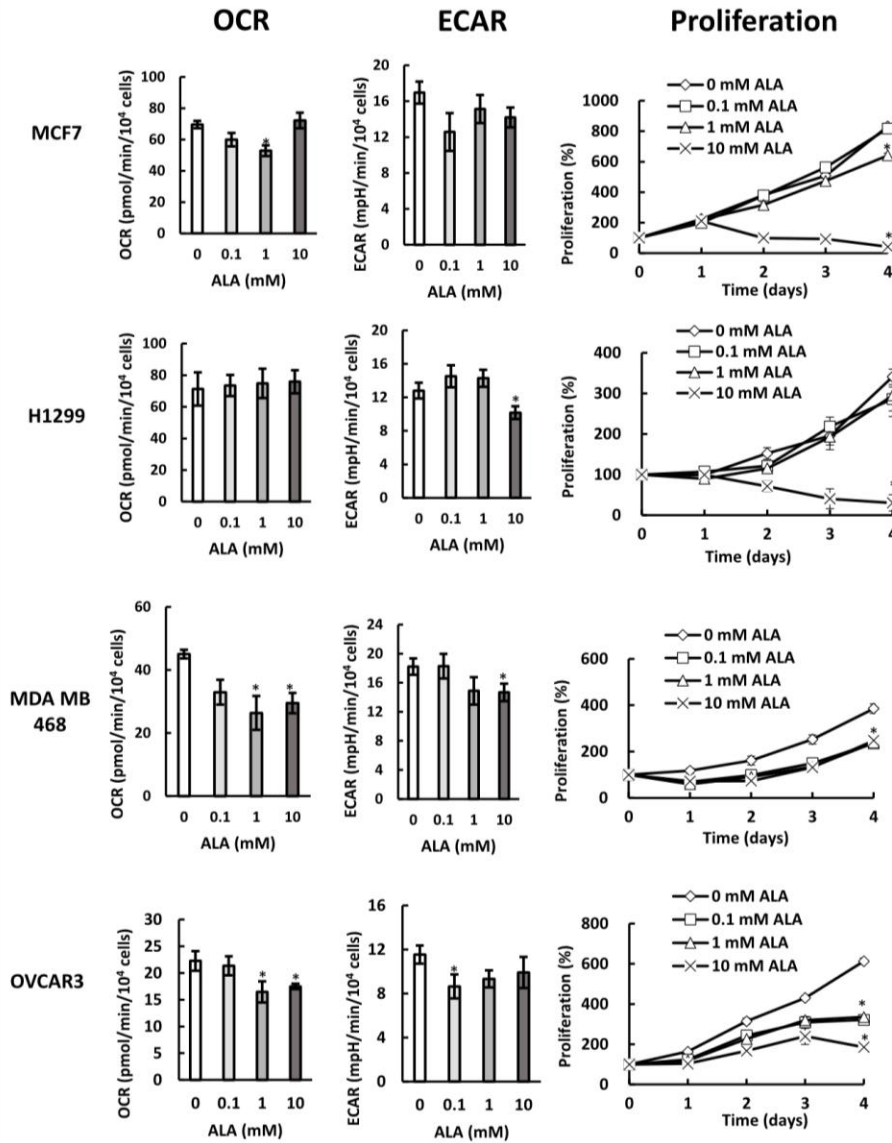


Figure 8. Cells with different activities of aerobic metabolism display unique patterns of ALA sensitivity.

OCR, ECAR, and proliferation in breast cancer MCF7 cells, lung cancer H1299 cells, TNBC cells MDA MB 468, and ovarian cancer OVCAR3 cells.

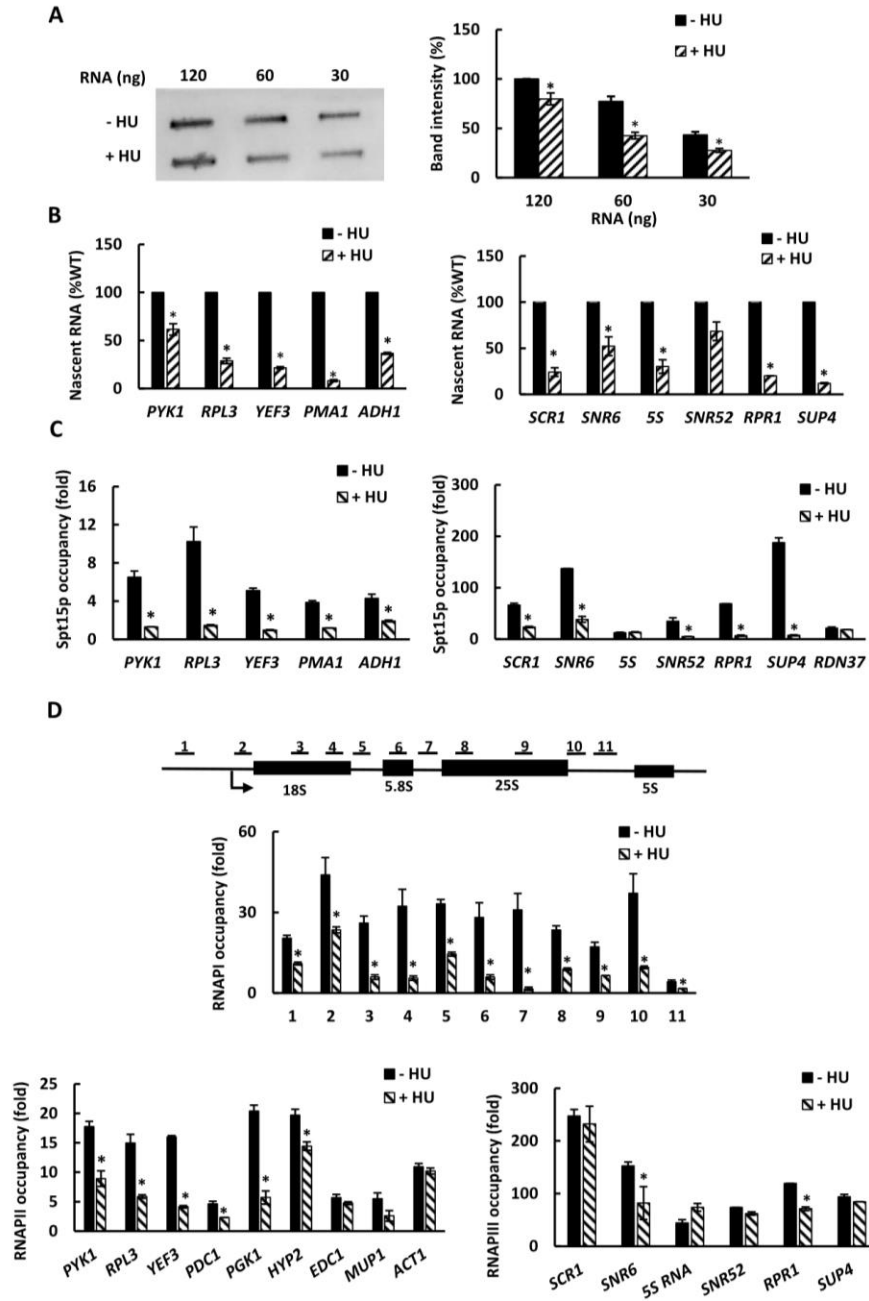


Figure 9. HU globally inhibits RNA synthesis and transcription by RNAPI, II, and III.

(A) Slot blot analysis of RNA isolated from WT cells (W303-1a) before and after treatment with 200 mM hydroxyurea (HU) for 30 min. The figure represents typical results from three independent experiments. The right panel shows quantitative analysis of the slot blot. The intensity of each band was quantified by densitometry and the results were normalized to untreated WT cells. (B) Nascent RNA levels of genes transcribed by RNAPII (left panel) and RNAPIII (right panel) in WT cells before and after treatment with 200 mM HU for 30 min. The results are expressed relative to the value for the WT strain and are normalized to *S. pombe* tubulin mRNA. The experiments were repeated three times, and the results are shown as the means \pm SD. (C) Occupancies of Spt15p in WT cells expressing *SPT15* tagged with three copies of the HA epitope (strain AD066) before and after treatment with 200 mM HU for 15 min at genes transcribed by RNAPII (left panel) and RNAPI and RNAPIII (right panel). (D) Occupancies of RNAPI (strain JS311-A190MN), RNAPII (strain W303-1a), and RNAPIII (strain RET1-13MYC) at highly transcribed genes before and after treatment with 200 mM HU for 15 min. (C, D) each immunoprecipitation was performed at least three times using different chromatin samples, and the occupancy at the indicated genes was calculated using the *POLI* coding sequence as a negative control. The data are presented as fold occupancy over the *POLI* coding sequence control and represent the means \pm SD. (A-D) Values for the HU-treated samples that are statistically different ($p < 0.05$) from values for the untreated samples in the same strain are indicated by an asterisk.

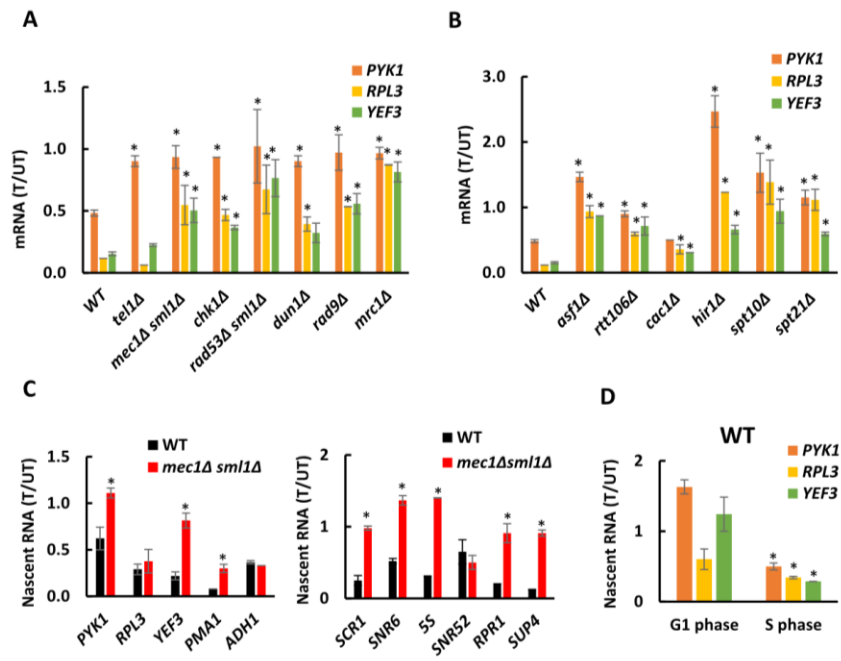


Figure 10. The transcriptional effect of HU is attenuated in checkpoint and chromatin mutants.

mRNA levels remaining after treatment with 200 mM hydroxyurea (HU) for 30 min, calculated as a ratio of mRNA levels in treated (T)/untreated (UT) samples for (A) WT (W303-1a), *tel1* Δ (SN159), *mec1* Δ *sml1* Δ (SN117), *chk1* Δ (SN136), *rad53* Δ *sml1* Δ (LG606), *dun1* Δ (SN141), *rad9* Δ (SJ027) and *mrc1* Δ (SJ015) cells, and (B) WT (W303-1a), *rtt106* Δ (MZ642), *rtt109* Δ (MZ655), *hir1* Δ (MZ700), *cac1* Δ (MZ553), and *asf1* Δ (MZ576) cells. The results were normalized to *RDN25* RNA. (C, D) Nascent mRNA levels remaining after 30 min HU treatment, calculated as a ratio of nascent mRNA levels in treated (T)/untreated (UT) samples for (C) WT (W303-1a) and *mec1* Δ *sml1* Δ (SN117) cells and (D) WT (W303-1a) cells arrested with α -factor in G1-phase and subsequently released into S-phase. The results were normalized to *S. pombe* tubulin mRNA. (A-D) The experiments were repeated three times, and the results are shown as the means \pm SD. (A, B, C) Values for the mutant strains that are statistically different ($p < 0.05$) from values for the WT strain are indicated by an asterisk. (D) Values for S phase cells that are statistically different ($p < 0.05$) from values for G1 phase cells are indicated by an asterisk.

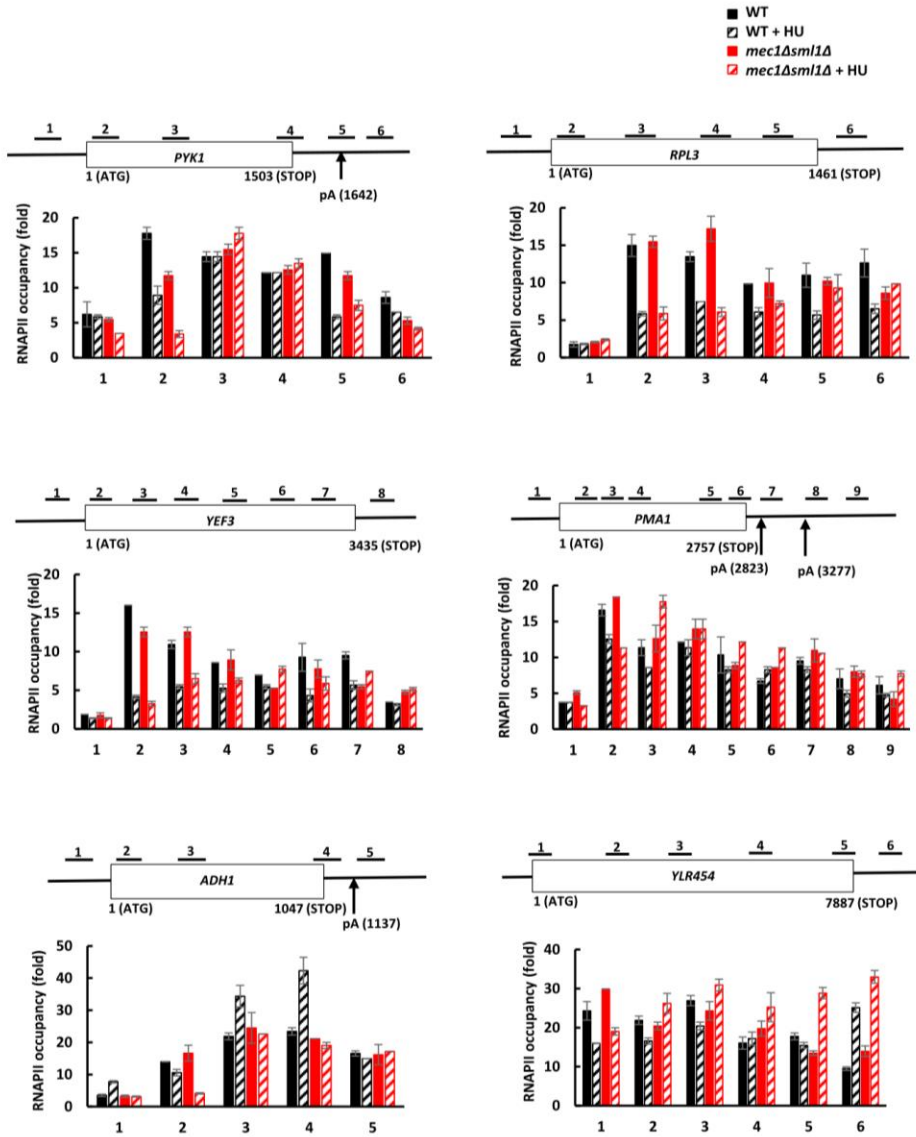


Figure 11. HU removes RNAPII from chromatin in a gene-specific manner.

Occupancies of RNPII across *PYK1*, *RPL3*, *YEF3*, *PMA1*, *ADH1*, and *YLR454* genes before and after treatment with 200 mM hydroxyurea (HU) for 15 min in WT (W303-1a, SN691) and *mec1Δsml1Δ* (SN117, SN684) cells. For ChIP analysis of *PYK1*, *RPL3*, *YEF3*, *PMA1*, and *ADH1* genes, cells were grown in YPD medium. For analysis of *YLR454* gene, WT or *mec1Δsml1Δ* cells containing *GALI::YLR454* construct (SN691 and SN684) were grown in YP medium with 2% raffinose and the expression of *YLR454* was induced for 2 h with 2% galactose. The top diagram of each gene shows schematic representation of the primers used in ChIP analysis. The positions of the polyadenylation sites (pA) in *PYK1*, *PMA1*, and *ADH1* are according to (110,119). Each immunoprecipitation was performed at least three times using different chromatin samples, and the occupancy at the indicated genes was calculated using the *POL1* coding sequence as a negative control. The data are presented as fold occupancy over the *POL1* coding sequence control and represent the means \pm SD.

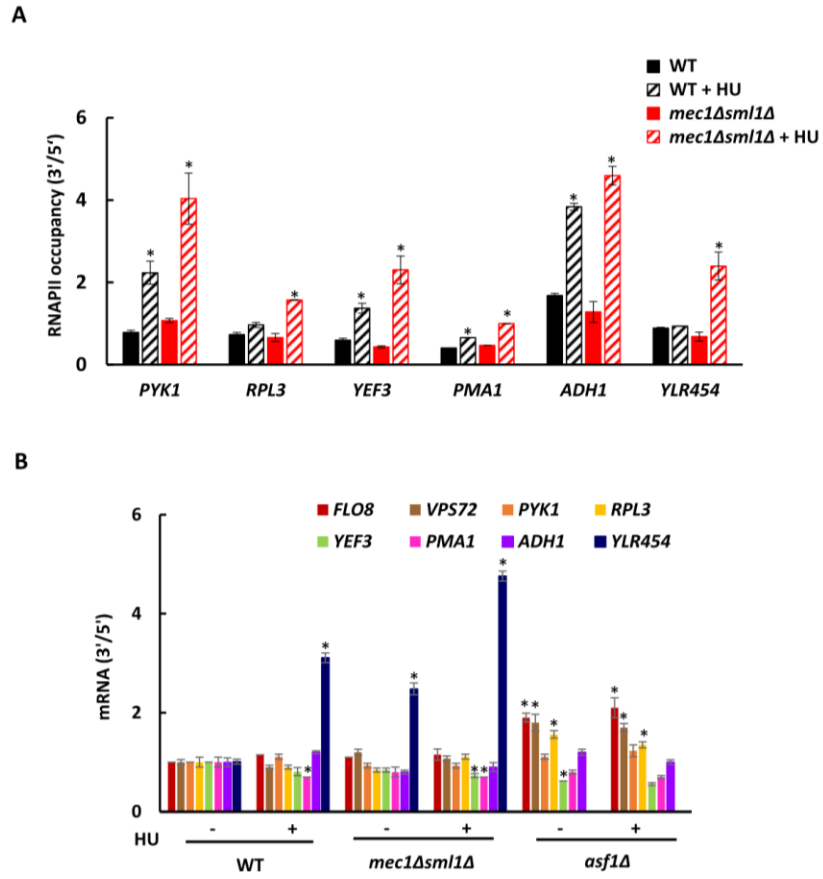


Figure 12. HU triggers RNAPII accumulation in 3' end of genes.

(A) Ratio of RNAPII occupancies at 3' and 5' ends of *PYK1*, *RPL3*, *YEF3*, *PMAI*, *ADHI*, and *YLR454* genes before and after HU treatment for 15 min in WT (W303-1a) and *mec1Δsml1Δ* (SN117) cells. The ratios were calculated using values from Fig. 11 that correspond to the following ChIP primer positions in *PYK1* (2, 4), *RPL3* (2, 5), *YEF3* (2, 7), *PMAI* (2, 6), *ADHI* (2, 4), and *YLR454* (1, 5). Values for the treated cells that are statistically different ($p < 0.05$) from the values for the corresponding untreated strain are indicated by an asterisk. (B) Ratios of mRNA levels at 3' and 5' ends of the indicated genes before and after HU treatment in WT (W303-1a), *mec1Δsml1Δ* (SN117) and *asf1Δ* (MZ576) cells. The results were normalized to *RDN25* RNA. The experiments were repeated three times, and the results are shown as the means \pm SD. Values that are statistically different ($p < 0.05$) from values for untreated WT strain are indicated by an asterisk.

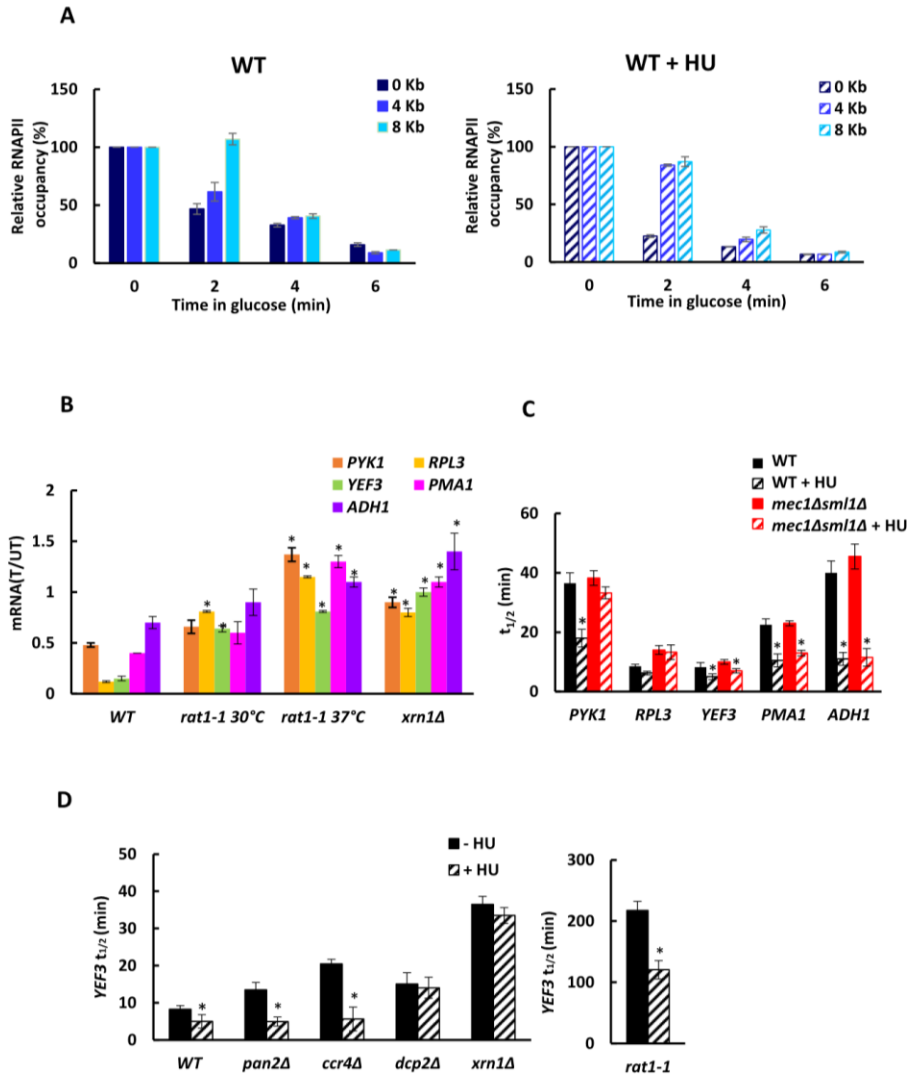


Figure 13. HU destabilizes mRNAs.

(A) Transcription elongation rate assay. WT cells containing *GALI::YLR454* construct (SN691) were grown in YP medium with 2% raffinose to an $A_{600\text{nm}} \sim 0.4$ and then induced with 2% galactose for 2 hours. Subsequently, 2% glucose was added to stop transcription and Rbp1p occupancies were determined after 0, 2, 4, and 6 min. at 0, 4, and 8 kb. Each immunoprecipitation was performed at least three times using different chromatin samples, and the occupancy at the indicated positions was calculated using the *POL1* coding sequence as a negative control. The data was calculated as a percentage relative to the occupancy at 0 min and represent the means \pm SD. (B) mRNA levels remaining after 30 min HU treatment, calculated as a ratio of mRNA levels in treated (T)/untreated (UT) samples for WT (W303-1a), *rat1-1* (YSB1796) cells grown at 30°C, *rat1-1* cells grown at 30°C and shifted to 37°C for 1h, and *xrn1* Δ (MB115) cells. The results were normalized to *RDN25* RNA. Values for the mutant strains that are statistically different ($p < 0.05$) from values for the WT strain are indicated by an asterisk. (C) Half-lives of mRNAs ($t_{1/2}$) in WT (W303-1a) and *mec1* Δ *sml1* Δ (SN117) cells before and after HU treatment for 30 min. (D) Half-lives of *YEF3* mRNA ($t_{1/2}$) in WT (W303-1a), *pan2* Δ (MB123), *ccr4* Δ (SM096), *dcp2* Δ (MB129), *xrn1* Δ (MB115), and *rat1-1* Δ (YSB1796) cells before and after HU treatment for 30 min. (C, D) Values for the HU treated samples that are statistically different ($p < 0.05$) from values for the untreated samples in the same strain are indicated by an asterisk. (A-E) The experiments were repeated three times, and the results are shown as the means \pm SD.

REFERENCES

1. Vander, Heiden M.G., DeBerardinis, R.J. (2017) Understanding the intersections between metabolism and cancer biology. *Cell* **168**, 657-669.
2. Vander Heiden, M.G., Cantley L.C., Thompson C.B. (2009) Understanding the Warburg effect: The metabolic requirements of cell proliferation. *Science* **324**, 1029-1033.
3. Földi, M., Stickeler, E., Bau, L., Kretz, O., Watermann, D., Gitsch, G., *et al.* (2017) Transketolase protein TKTL1 overexpression: A potential biomarker and therapeutic target in breast cancer. *Oncol Rep.* **17**, 841-845.
4. Langbein, S., Zerilli, M., Zur Hausen, A., Staiger, W., Rensch-Boschert, K., Lukan, N., *et al.* (2006) Expression of transketolase TKTL1 predicts colon and urothelial cancer patient survival: Warburg effect reinterpreted. *Br J Cancer* **94**, 578-585.
5. Wang, H.Q., Altomare, .A., Skele, K.L., Poulikakos, P.I., Kuha, F.P., Di Cristofano, A., *et al.* (2005) Positive feedback regulation between AKT activation and fatty acid synthase expression in ovarian carcinoma cells. *Oncogene* **24**, 3574-3582.
6. Glunde, K., Bhujwala, Z.M. (2007) Choline kinase alpha in cancer prognosis and treatment. *Lancet Oncol.* **8**, 855-857.
7. Birsoy, K., Wang, T., Chen, W.W., Freinkman, E., Abu-Remaileh, M., Sabatini, D.M. (2015) An essential role of the mitochondrial electron transport chain in cell proliferation is to enable aspartate synthesis. *Cell* **162**, 540-551.
8. Sullivan, L.B., Gui, D.Y., Hosios, A.M., Bush, L.N., Freinkman, E., Vander Heiden, M.G. (2015) Supporting aspartate biosynthesis is an essential function of respiration in proliferating cells. *Cell* **162**, 552-563.

9. Sciacovelli, M., Gaude, E., Hilvo, M., Frezza, C. (2014) The metabolic alterations of cancer cells. *Methods Enzymol.* **542**, 1-23.
10. Dong, L., Gopalan, V., Holland, O., Neuzil, J. (2020) Mitocans Revisited: Mitochondrial Targeting as Efficient Anti-Cancer Therapy. *Int J Mol Sci.* **21**, 7941.
11. Kankotia, S., Stacpoole, P.W. (2014) Dichloroacetate and cancer: New home for an orphan drug? *Biochim Biophys Acta.* **1846**, 617-629.
12. Kim, J.W., Tchernyshyov, I., Semenza, G.L., Dang, C.V. (2006) HIF-1-mediated expression of pyruvate dehydrogenase kinase: a metabolic switch required for cellular adaptation to hypoxia. *Cell Metab.* **3**, 177-185.
13. Papandreou, I., Cairns, R.A., Fontana, L., Lim, A.L., Denko, N.C. (2006) HIF-1 mediates adaptation to hypoxia by actively downregulating mitochondrial oxygen consumption. *Cell Metab.* **3**, 187-197.
14. Pouyssegur, J., Dayan, F., Mazure, N.M. (2006) Hypoxia signalling in cancer and approaches to enforce tumour regression. *Nature* **441**, 437-443.
15. Weinberg, S.E., Chandel, N.S. (2015) Targeting mitochondria metabolism for cancer therapy. *Nat Chem Biol.* **11**, 9-15.
16. Vancura, A., Bu, P., Bhagwat, M., Zeng, J., Vancurova, I. (2018) Metformin as an Anticancer Agent. *Trends Pharmacol Sci.* **39**, 867-878.
17. Mense, S.M., Zhang, L. (2006) Heme: a versatile signaling molecule controlling the activities of diverse regulators ranging from transcription factors to MAP kinases. *Cell Res.* **16**, 681-692.
18. Ogura, S., Maruyama, K., Hagiya, Y., Sugiyama, Y., Tsuchiya, K., Takahashi, K., Abe, F., Tabata, K., Okura, I., Nakajima, M., and Tanaka, T. (2011) The effect of 5-aminolevulinic acid on cytochrome c oxidase activity in mouse liver. *BMC Res Notes.* **4**, 66.

19. Sugiyama, Y., Hagiya, Y., Nakajima, M., Ishizuka, M., Tanaka, T., Ogura, S. (2014) The heme precursor 5-aminolevulinic acid disrupts the Warburg effect in tumor cells and induces caspase-dependent apoptosis. *Oncol Rep.* **31**, 1282-1286.
20. Sohoni, S., Ghosh, P., Wang, T., Kalainayakan, S.P., Vidal, C., Dey, S., *et al.* (2019) Elevated Heme Synthesis and Uptake Underpin Intensified Oxidative Metabolism and Tumorigenic Functions in Non-Small Cell Lung Cancer Cells. *Cancer Res.* **79**, 2511-2525.
21. Zhang, T., Bu, P., Zeng, J., Vancura, A. (2017) Increased heme synthesis in yeast induces a metabolic switch from fermentation to respiration even under conditions of glucose repression. *J. Biol. Chem.* **292**, 16942-16954.
22. Gozzelino, R., Jeney, V., Soares, M.P. (2010) Mechanisms of cell protection by heme oxygenase-1. *Annu. R. Pharmacol. Toxicol.* **50**, 323-354.
23. Laafi, J., Homedan, C., Jacques, C., Gueguen, N., Schmitt, C., Puy, H., *et al.* (2014) Pro-oxidant effect of ALA is implicated in mitochondrial dysfunction of HepG2 cells. *Biochimie.* **106**, 157-166.
24. Wiel, C., Le Gal, K., Ibrahim, M.X., Jahangir, C.A., Kashif, M., Yao, H., *et al.* (2019) BACH1 Stabilization by Antioxidants Stimulates Lung Cancer Metastasis. *Cell* **178**, 330-345.
25. Lignitto, L., LeBoeuf, S.E., Homer, H., Jiang, S., Askenazi, M., Karakousi, T.R., *et al.* (2019) Nrf2 Activation Promotes Lung Cancer Metastasis by Inhibiting the Degradation of Bach1. *Cell* **17**, 316-329.
26. Lee, J., Yesilkanal, A.E., Wynne, J.P., Frankenberger, C., Liu, J., Yan, J., *et al.* (2019) Effective breast cancer combination therapy targeting BACH1 and mitochondrial metabolism. *Nature* **568**, 254-258.
27. Lee, U., Frankenberger, C., Yun, J., Bevilacqua, E., Caldas, C., Chin, S.F., *et al.* (2013) A prognostic gene signature for metastasis-free survival of triple negative breast cancer patients. *PLoS One* **8**, e82125.

28. Liang, Y., Wu, H., Lei, R., Chong, R.A., Wei, Y., Lu, X., *et al.* (2012) Transcriptional network analysis identifies BACH1 as a master regulator of breast cancer bone metastasis. *J Biol Chem.* **287**, 33533-33544.
29. Yun, J., Frankenberger, C.A., Kuo, W.L., Boelens, M.C., Eves, E.M., Cheng, N., *et al.* (2017) Signaling pathway for RKIP and Let-7 regulates and predicts metastatic breast cancer. *EMBO J.* **30**, 4500-4514.
30. Zenke-Kawasaki, Y., Dohi, Y., Katoh, Y., Ikura, T., Ikura, M., Asahara, *et al.* (2007) Heme induces ubiquitination and degradation of the transcription factor Bach1. *Mol Cell Biol* **27**, 6962-6971.
31. Zou, Y., Uddin, M.M., Padmanabhan, S., Zhu, Y., Bu, P., Vancura, A., *et al.* (2018) The proto-oncogene Bcl3 induces immune checkpoint PD-L1 expression, mediating proliferation of ovarian cancer cells. *J Biol Chem.* **293**, 15483-15496.
32. Gaire, B., Uddin, M.M., Zou, Y., Vancurova, I. (2020) Analysis of IFN γ -Induced Migration of Ovarian Cancer Cells. *Methods Mol Biol.* **2108**, 101-106.
33. Kaur, P., Nagar, S., Bhagwat, M., Uddin, M.M., Zhu, Y., Vancura, A. (2020) Probing Metabolic Changes in IFN γ -Treated Ovarian Cancer Cells. *Methods Mol Biol.* **2108**, 197-207.
34. Singha, B., Gatla, H.R., Manna, S., Chang, T.P., Sanacora, S., Poltoratsky, V., *et al.* (2014) Proteasome inhibition increases recruitment of I κ B kinase β (IKK β), S536P-p65, and transcription factor EGR1 to interleukin-8 (IL-8) promoter, resulting in increased IL-8 production in ovarian cancer cells. *J Biol Chem* **289**, 2687-2700.
35. Galdieri, L., Gatla, H., Vancurova, I., Vancura, A. (2016) Activation of AMP-activated Protein Kinase by Metformin Induces Protein Acetylation in Prostate and Ovarian Cancer Cells. *J Biol Chem.* **291**, 25154-25166.
36. Hardie, D.G. (2011) AMP-activated protein kinase: an energy sensor that regulates all aspects of cell function. *Genes Dev.* **25**, 1895-1908.

37. Ha, J., Daniel, S., Broyles, S.S., Kim, K.H. (1994) Critical phosphorylation sites for acetyl-CoA carboxylase activity. *J Biol Chem.* **269**, 22162-22168.
38. Padilla, J., Lee, J. (2021) A novel therapeutic target, BACH1, regulates cancer metabolism. *Cells* **10**, 634.
39. Pamplona, A., Ferreira, A., Balla, J., Jeney, V., Balla, G., Epiphonio, S., *et al.* (2007) Heme oxygenase-1 and carbon monoxide suppress the pathogenesis of experimental cerebral malaria. *Nat Med.* **13**, 703-710.
40. Heinemann, I.U., Jahn, M., Jahn, D. (2008) The biochemistry of heme biosynthesis. *Arch. Biochem. Biophys.* **474**, 238-251.
41. Fukuda, H., Casas, A., Batlle, A. (2005) Aminolevulinic acid: from its unique biological function to its star role in photodynamic therapy. *Int J Biochem Cell Biol.* **37**, 272-276.
42. Buytaert, E., Dewaele, M., Agostinis, P. (2007) Molecular effectors of multiple cell death pathways initiated by photodynamic therapy. *Biochim Biophys Acta.* **1776**, 86-107.
43. Ishizuka, M., Abe, F., Sano, Y., Takahashi, K., Inoue, K., Nakajima, *et al.* (2011) M. Novel development of 5-aminolevulinic acid (ALA) in cancer diagnoses and therapy. *Int Immunopharmacol.* **11**, 358-365.
44. Sies, H., Berndt, C., Jones, D.P. (2017) Oxidative Stress. *Annu Rev Biochem.* **86**, 715-748.
45. Chio, IIC., Tuveson, D.A. (2017) ROS in Cancer: The Burning Question. *Trends Mol Med.* **23**, 411-429.
46. Perillo, B., Di Donato, M., Pezone A., Di Zazzo, E., Giovannelli, P., Galasso, G., *et al.* (2020) ROS in cancer therapy: the bright side of the moon. *Exp. Mol. Med.* **52**, 192-203

47. Sancar, A., Lindsey-Boltz, L.A., Unsal-Kacmaz, K., and Linn, S. (2004) Molecular mechanisms of mammalian DNA repair and the DNA damage checkpoints. *Annu. Rev. Biochem.* **73**, 39-85
48. Putnam, C.D., Jaehnig, E.J., and Kolodner, R.D. (2009) Perspectives on the DNA damage and replication checkpoint responses in *Saccharomyces cerevisiae*. *DNA Repair* **8**, 974-982
49. Ciccía, A., and Elledge, S.J. (2010) The DNA damage response: making it safe to play with knives. *Mol. Cell* **40**, 179-204
50. Kolodner, R.D., Putnam, C.D., and Myung, K. (2002) Maintenance of genome stability in *Saccharomyces cerevisiae*. *Science* **297**, 552-557
51. Putnam, C.D., and Kolodner, R.D. (2017) Pathways and mechanisms that prevent genome instability in *Saccharomyces cerevisiae*. *Genetics* **206**, 1187-1225
52. Bell, S.P., and Labib, K. (2016) Chromosome Duplication in *Saccharomyces cerevisiae*. *Genetics* **203**, 1027–1067
53. Pardo, B., Crabbé, L., and Pasero, P. (2017) Signaling pathways of replication stress in yeast. *FEMS Yeast Res.* **17**
54. Lagerwerf, S., Vrouwe, M.G., Overmeer, R.M., Fousteri, M.I., and Mullenders, L.H. (2011) DNA damage response and transcription. *DNA Repair* **10**, 743–750
55. Giono, L.E., Nieto Moreno, N., Cambindo Botto, A.E., Dujardin, G., Muñoz, M.J., and Kornblihtt, A.R. (2016) The RNA Response to DNA Damage. *J. Mol. Biol.* **428**, 2636–2651
56. Capozzo, I., Iannelli, F., Francia, S., and d'Adda di Fagagna, F., (2017) Express or repress? The transcriptional dilemma of damaged chromatin. *FEBS J.* **284**, 2133-2147

57. Gregersen, L.H., and Svejstrup, J.Q. (2018) The Cellular Response to Transcription-Blocking DNA Damage. *Trends Biochem. Sci.* **43**, 327–341
58. Silva, E., and Ideker, T. (2019) Transcriptional responses to DNA damage. *DNA Repair* **79**, 40–49
59. Chardon, R., Muguet, A., Griesenbeck, J., Smerdon, M.J., and Conconi, A. (2019) In yeast cells arrested at the early S-phase by hydroxyurea, rRNA gene promoters and chromatin are poised for transcription while rRNA synthesis is compromised. *Mutat. Res.* **815**, 20–29
60. Bhalla, P., Shukla, A., Vernekar, D.V., Arimbasseri, A.G., Sandhu, K.S., and Bhargava, P. (2019) Yeast PAF1 complex counters the pol III accumulation and replication stress on the tRNA genes. *Sci. Rep.* **9**, 12892
61. Shanbhag, N.M., Rafalska-Metcalf, I.U., Balane-Bolivar, C., Janicki, S.M., and Greenberg, R.A. (2010) ATM-dependent chromatin changes silence transcription in cis to DNA double-strand breaks. *Cell* **141**, 970–981
62. Charlet-Berguerand, N., Feuerhahn, S., Kong, S.E., Ziserman, H., Conaway, J.W., Conaway, R., and Egly, J.M. (2006) RNA polymerase II bypass of oxidative DNA damage is regulated by transcription elongation factors. *EMBO J.* **25**, 5481–5491
63. Tufegdžić Vidaković, A., Mitter, R., Kelly, G.P., Neumann, M., Harreman, M., Rodríguez-Martínez, M., Herlihy, A., Weems, J.C., Boeing, S., Encheva, V., Gaul, L., Milligan, L., Tollervey, D., Conaway, R.C., Conaway, J.W., Snijders, A.P., Stewart, A., and Svejstrup, J.Q. (2020) Regulation of the RNAPII Pool Is Integral to the DNA Damage Response. *Cell* **180**, 1245–126

64. Nguyen, V.C., Clelland, B.W., Hockman, D.J., Kujat-Choy, S.L., Mewhort, H.E., and Schultz, M.C. (2010) Replication stress checkpoint signaling controls tRNA gene transcription. *Nat. Struct. Mol. Biol.* **17**, 976–981
65. Poli, J., Gerhold, C.B., Tosi, A., Hustedt, N., Seeber, A., Sack, R., Herzog, F., Pasero, P., Shimada, K., Hopfner, K.P., and Gasser, S.M. (2016) Mec1, INO80, and the PAF1 complex cooperate to limit transcription replication conflicts through RNAPII removal during replication stress. *Genes Dev.* **30**, 337–354
66. Hurst, V., Challa, K., Jonas, F., Forey, R., Sack, R., Seebacher, J., Schmid, C.D., Barkai, N., Shimada, K., Gasser, S.M., and Poli, J. (2021) A regulatory phosphorylation site on Mec1 controls chromatin occupancy of RNA polymerases during replication stress. *EMBO J.* **40**, E108439
67. Sidorova, J.M., and Breeden, L.L. (1997) Rad53-dependent phosphorylation of Swi6 and down-regulation of CLN1 and CLN2 transcription occur in response to DNA damage in *Saccharomyces cerevisiae*. *Genes Dev.* **11**, 3032–3045
68. Sidorova, J.M., and Breeden, L.L. (2003) Rad53 checkpoint kinase phosphorylation site preference identified in the Swi6 protein of *Saccharomyces cerevisiae*. *Mol. Cell Biol.* **23**, 3405–3416
69. Travesa, A., Kuo, D., de Bruin, R.A., Kalashnikova, T.I., Guaderrama, M., Thai, K., Aslanian, A., Smolka, M.B., Yates, J.R., 3rd, Ideker, T., and Wittenberg, C. (2012) DNA replication stress differentially regulates G1/S genes via Rad53-dependent inactivation of Nrm1. *EMBO J.* **31**, 1811–1822
70. Bastos de Oliveira, F.M., Harris, M.R., Brazauskas, P., de Bruin, R.A., and Smolka, M.B. (2012) Linking DNA replication checkpoint to MBF cell-cycle transcription reveals a distinct class of G1/S genes. *EMBO J.* **31**, 1798–1810

71. Jaehnig, E.J., Kuo, D., Hombauer, H., Ideker, T.G., and Kolodner, R.D. (2013) Checkpoint kinases regulate a global network of transcription factors in response to DNA damage. *Cell Rep.* **4**, 174–188
72. Zhou, C., Elia, A.E., Naylor, M.L., Dephoure, N., Ballif, B.A., Goel, G., Xu, Q., Ng, A., Chou, D.M., Xavier, R.J., Gygi, S.P., and Elledge, S.J. (2016) Profiling DNA damage-induced phosphorylation in budding yeast reveals diverse signaling networks. *Proc. Natl. Acad. Sci. U. S. A.* **113**, E3667-3675
73. Lavigne, M.D., Konstantopoulos, D., Ntakou-Zamplara, K.Z., Liakos, A., and Fousteri, M. (2017) Global unleashing of transcription elongation waves in response to genotoxic stress restricts somatic mutation rate. *Nat. Commun.* **8**, 2076
74. Williamson, L., Saponaro, M., Boeing, S., East, P., Mitter, R., Kantidakis, T., Kelly, G.P., Lobley, A., Walker, J., Spencer-Dene, B., Howell, M., Stewart, A., and Svejstrup, J.Q. (2017) UV Irradiation Induces a Non-coding RNA that Functionally Opposes the Protein Encoded by the Same Gene. *Cell* **168**, 843–855
75. Gyenis, A., Umlauf, D., Ujfaludi, Z., Boros, I., Ye, T., and Tora, L. (2014) UVB induces a genome-wide acting negative regulatory mechanism that operates at the level of transcription initiation in human cells. *PLoS Genet.* **10**, E1004483
76. Rockx, D.A., Mason, R., van Hoffen, A., Barton, M.C., Citterio, E., Bregman, D.B., van Zeeland, A.A., Vrieling, H., and Mullenders, L.H. (2000) UV-induced inhibition of transcription involves repression of transcription initiation and phosphorylation of RNA polymerase II. *Proc. Natl. Acad. Sci. U. S. A.* **97**, 10503–10508
77. Galli, A., and Schiestl, R. H. (1996). Hydroxyurea induces recombination in dividing but not in G1 or G2 cell cycle arrested yeast cells. *Mutation Res.* **354**, 69–75

78. Szikriszt, B., Póti, Á., Pipek, O., Krzystanek, M., Kanu, N., Molnár, J., Ribli, D., Szeltner, Z., Tusnády, G. E., Csabai, I., Szallasi, Z., Swanton, C., and Szüts, D. (2016) A comprehensive survey of the mutagenic impact of common cancer cytotoxics. *Genome Biol.* **17**, 99.
79. Zhao, X., Chabes, A., Domkin, V., Thelander, L., and Rothstein, R. (2001) The ribonucleotide reductase inhibitor Sml1 is a new target of the Mec1/Rad53 kinase cascade during growth and in response to DNA damage. *EMBO J.* **20**, 3544-3553
80. Pelechano, V., Chávez, S., and Pérez-Ortín, J.E. (2010) A complete set of nascent transcription rates for yeast genes. *PloS One* **5**, E15442
81. Bhagwat, M., Nagar, S., Kaur, P., Mehta, R., Vancurova, I., and Vancura, A. (2021) Replication stress inhibits synthesis of histone mRNAs in yeast by removing Spt10p and Spt21p from the histone promoters. *J. Biol. Chem.* **297**, 101246.
82. Kaplan, C.D., Laprade, L., and Winston, F. (2003) Transcription elongation factors repress transcription initiation from cryptic sites. *Science* **301**, 1096–1099
83. Keogh, M.C., Kurdistani, S.K., Morris, S.A., Ahn, S.H., Podolny, V., Collins, S.R., Schuldiner, M., Chin, K., Punna, T., Thompson, N.J., Boone, C., Emili, A., Weissman, J.S., Hughes, T.R., Strahl, B.D., Grunstein, M., Greenblatt, J.F., Buratowski, S., and Krogan, N.J. (2005) Cotranscriptional set2 methylation of histone H3 lysine 36 recruits a repressive Rpd3 complex. *Cell* **123**, 593–605
84. Carrozza, M.J., Li, B., Florens, L., Suganuma, T., Swanson, S.K., Lee, K.K., Shia, W.J., Anderson, S., Yates, J., Washburn, M.P., and Workman, J.L. (2005) Histone H3 methylation by Set2 directs deacetylation of coding regions by Rpd3S to suppress spurious intragenic transcription. *Cell* **123**, 581–592

85. Joshi, A.A., and Struhl, K. (2005) Eaf3 chromodomain interaction with methylated H3-K36 links histone deacetylation to Pol II elongation. *Mol. Cell* **20**, 971–978
86. Cheung, V., Chua, G., Batada, N.N., Landry, C.R., Michnick, S.W., Hughes, T.R., and Winston, F. (2008) Chromatin- and transcription-related factors repress transcription from within coding regions throughout the *Saccharomyces cerevisiae* genome. *PLoS Biol.* **6**, E277
87. Schwabish, M.A., and Struhl, K. (2006) Asf1 mediates histone eviction and deposition during elongation by RNA polymerase II. *Mol. Cell* **22**, 415–422
88. Mason, P.B., and Struhl, K. (2005) Distinction and relationship between elongation rate and processivity of RNA polymerase II in vivo. *Mol. Cell* **17**, 831–840
89. Parker R. (2012) RNA degradation in *Saccharomyces cerevisiae*. *Genetics* **191**, 671-702
90. Lykke-Andersen, S., and Jensen, T.H. (2007) Overlapping pathways dictate termination of RNA polymerase II transcription. *Biochimie* **89**, 1177–1182
91. Mischo, H.E., and Proudfoot, N.J. (2013) Disengaging polymerase: terminating RNA polymerase II transcription in budding yeast. *Biochim. Biophys. Acta.* **1829**, 174–185
92. Baejen, C., Andreani, J., Torkler, P., Battaglia, S., Schwalb, B., Lidschreiber, M., Maier, K.C., Boltendahl, A., Rus, P., Esslinger, S., Söding, J., and Cramer, P. (2017) Genome-wide Analysis of RNA Polymerase II Termination at Protein-Coding Genes. *Mol. Cell* **66**, 38–49

93. Tudek, A., Lloret-Llinares, M., and Jensen, T.H. (2018) The multitasking polyA tail: nuclear RNA maturation, degradation and export. *Philos. Trans. R. Soc. Lond. B. Biol. Sci.* **373**, 20180169
94. Luo, W., and Bentley, D. (2004) A ribonucleolytic rat torpedo RNA polymerase II. *Cell* **119**, 911–914
95. Luo, W., Johnson, A.W., and Bentley, D.L. (2006) The role of Rat1 in coupling mRNA 3'-end processing to transcription termination: implications for a unified allosteric-torpedo model. *Genes Dev.* **20**, 954–965
96. Hyman, L. E., & Moore, C. L. (1993) Termination and pausing of RNA polymerase II downstream of yeast polyadenylation sites. *Mol. Cell. Biol.* **13**, 5159–5167
97. Gaillard, H., and Aguilera, A. (2014) Cleavage factor I links transcription termination to DNA damage response and genome integrity maintenance in *Saccharomyces cerevisiae*. *PLoS Genet.* **10**, E1004203
98. Kuehner, J.N., Kaufman, J.W., and Moore, C. (2017) Stimulation of RNA Polymerase II ubiquitination and degradation by yeast mRNA 3'-end processing factors is a conserved DNA damage response in eukaryotes. *DNA Repair* **57**, 151–160
99. Dutertre, M., Sfaxi, R., and Vagner, S. (2021) Reciprocal Links between Pre-messenger RNA 3'-End Processing and Genome Stability. *Trends Biochem. Sci.* **46**, 579–594
100. Graber, J.H., Nazeer, F.I., Yeh, P.C., Kuehner, J.N., Borikar, S., Hoskinson, D., and Moore, C.L. (2013) DNA damage induces targeted, genome-wide variation of poly(A) sites in budding yeast. *Genome Res.* **23**, 1690-1703

101. Casañal, A., Kumar, A., Hill, C.H., Easter, A.D., Emsley, P., Degliesposti, G., Gordiyenko, Y., Santhanam, B., Wolf, J., Wiederhold, K., Dornan, G.L., Skehel, M., Robinson, C.V., and Passmore, L.A. (2017) Architecture of eukaryotic mRNA 3'-end processing machinery. *Science* **358**, 1056–1059
102. Kühn, U., Gündel, M., Knoth, A., Kerwitz, Y., Rüdell, S., and Wahle, E. (2009) Poly(A) tail length is controlled by the nuclear poly(A)-binding protein regulating the interaction between poly(A) polymerase and the cleavage and polyadenylation specificity factor. *J. Biol. Chem.* **284**, 22803–22814
103. Stewart M. (2019) Polyadenylation and nuclear export of mRNAs. *J. Biol. Chem.* **294**, 2977–2987
104. Turtola, M., Manav, M.C., Kumar, A., Tudek, A., Mroczek, S., Krawczyk, P.S., Dziembowski, A., Schmid, M., Passmore, L.A., Casañal, A., and Jensen, T.H. (2021) Three-layered control of mRNA poly(A) tail synthesis in *Saccharomyces cerevisiae*. *Genes Dev.* **35**, 1290–1303
105. Bu, P., Nagar, S., Bhagwat, M., Kaur, P., Shah, A., Zeng, J., Vancurova, I., and Vancura, A. (2019) DNA damage response activates respiration and thereby enlarges dNTP pools to promote cell survival in budding yeast. *J. Biol. Chem.* **294**, 9771-9786
106. Demczuk, A., Guha, N., Nguyen, P.H., Desai, P., Chang, J., Guzinska, K., Rollins, J., Ghosh, C.C., Goodwin, L., and Vancura, A. (2008) *Saccharomyces cerevisiae* phospholipase C regulates transcription of Msn2p-dependent stress-responsive genes. *Eukaryot. Cell* **7**, 967-979
107. Mehrotra, S., Galdieri, L., Zhang, T., Zhang, M., Pemberton, L. F., & Vancura, A. (2014) Histone hypoacetylation-activated genes are repressed by acetyl-CoA- and chromatin-mediated mechanism. *Biochim. Biophys. Acta.* **1839**, 751–763

108. Galdieri, L., Zhang, T., Rogerson, D., and Vancura, A. (2016) Reduced Histone Expression or a Defect in Chromatin Assembly Induces Respiration. *Mol. Cell. Biol.* **36**, 1064-1077
109. Wong, C. M., Qiu, H., Hu, C., Dong, J., and Hinnebusch, A. G. (2007). Yeast cap binding complex impedes recruitment of cleavage factor IA to weak termination sites. *Mol. Cell. Biol.* **27**, 6520–6531
110. Kim, M., Krogan, N. J., Vasiljeva, L., Rando, O. J., Nedeá, E., Greenblatt, J. F., & Buratowski, S. (2004) The yeast Rat1 exonuclease promotes transcription termination by RNA polymerase II. *Nature* **432**, 517–522
111. Soragni, E., & Kassavetis, G. A. (2008). Absolute gene occupancies by RNA polymerase III, TFIIB, and TFIIC in *Saccharomyces cerevisiae*. *J. Biol. Chem.* **283**, 26568–26576.
112. Sherman, F. (1991) Getting started with yeast. *Methods Enzymol.* **194**, 3-21
113. Baptista, T., Grünberg, S., Minoungou, N., Koster, M., Timmers, H., Hahn, S., Devys, D., and Tora, L. (2018) SAGA Is a General Cofactor for RNA Polymerase II Transcription. *Mol. Cell* **70**, 1163–1164
114. Baptista, T. and Devys, D. (2018) *Saccharomyces cerevisiae* metabolic labeling with 4-thiouracil and the quantification of newly synthesized mRNA as a proxy for RNA polymerase II activity. *J. Vis. Exp.* **140**, e57982
115. Rädle, B., Rutkowski, A.J., Ruzsics, Z., Friedel, C.C., Koszinowski, U.H., and Dölken, L. (2013) Metabolic labeling of newly transcribed RNA for high resolution gene expression profiling of RNA synthesis, processing and decay in cell culture. *J. Vis. Exp.* **78**, 50195
116. Galdieri, L., and Vancura, A. (2012) Acetyl-CoA carboxylase regulates global histone acetylation. *J. Biol. Chem.* **287**, 23865-23876

117. Collier, J. (2008) Methods to determine mRNA half-life in *Saccharomyces cerevisiae*. *Methods Enzymol.* **448**, 267-284
118. Passos, D.O., and Parker, R. (2008) Analysis of cytoplasmic mRNA decay in *Saccharomyces cerevisiae*. *Methods Enzymol.* **448**, 409-427
119. Kim, M., Ahn, S. H., Krogan, N. J., Greenblatt, J. F., & Buratowski, S. (2004) Transitions in RNA polymerase II elongation complexes at the 3' ends of genes. *EMBO J.* **23**, 354–364

Vita

Name	Pritpal Kaur
Baccalaureate Degree	<i>Bachelor of Science, Sri Guru Granth Sahib World University, Punjab, India Major: Biotechnology</i>
Date Graduated	<i>August, 2016</i>
Other Degrees and Certificates	<i>Master of Science, Sri Guru Granth Sahib World University, Punjab, India Major: Biotechnology</i>
Date Graduated	<i>August, 2017</i>